Quantum-critical properties of random transverse-field Ising models extracted by quantum Monte Carlo methods

Master's Thesis in Physics

Presented by
Calvin Christoph Krämer
30.11.2022

Institute for Theoretical Physics I
Friedrich-Alexander-Universität Erlangen-Nürnberg

Supervisor: Prof. Dr. Kai Phillip Schmidt

Abstract: The transverse-field Ising model with quenched disorder is studied in one and two dimensions at zero temperature by stochastic series expansion quantum Monte Carlo simulations. Using a sample-replication method we are able to determine distributions of pseudo-critical points, from which critical shift and width exponents $\nu_{s/w}$ are extracted by finite-size scaling. The scaling of the averaged magnetisation at the critical point is used further to determine the order-parameter critical exponent β. In one-dimensional systems our results agree well with literature. In two dimensions our results for $\nu_{s/w}$ are also in agreement with strong disorder renormalisation group studies, although not with high accuracy. The dynamical scaling in the Griffiths phase is investigated by measuring the local susceptibility in the disordered phase and the critical exponent z' is extracted.

Kurzzusammenfassung: Das Ising-Modell im transversalen Feld mit statischer Unordnung wird in ein und zwei Dimensionen bei Temperatur $T = 0$ mit der Stochastic Series Expansion Quanten Monte Carlo Methode untersucht. Mithilfe von Verteilungen von pseudokritischen Punkten werden kritische Exponenten $\nu_{s/w}$ für den Mittelwert und die Breite der Verteilung durch Finite-Size-Scaling extrahiert. Außerdem wird das Verhalten der gemittelten Magnetisierung am Punkt des Phasenübergangs zur Bestimmung des kritischen Exponenten β des Ordnungsparameters verwendet. In eindimensionalen Systemen stimmen unsere Ergebnisse gut mit der Literatur überein. In zweidimensionalen Systemen sind unsere Ergebnisse für $\nu_{s/w}$, wenn auch mit weniger Genauigkeit, ebenfalls konsistent mit anderen Arbeiten, die Strong Disorder Renormalisation Group Methoden verwendet haben. Um das dynamische Verhalten in der Griffiths-Phase zu untersuchen, wird die lokale Suszeptibilität in der ungeordneten Phase bestimmt und der kritischen Exponent z' extrahiert.

Contents

1 Introduction

To a certain extent, a perfect lattice structure is a good model for solids and brings advantages such as translational symmetry that make a mathematical description easier. In fact, modern solid-state physics is built on a periodic, uniform lattice structure. A disorder-free lattice serves as a model for many groundbreaking theorems describing solids. These include fundamental concepts such as Bloch's theorems or the work of Debye, Brillouin and others on the description of electronic band structures and lattice vibrations in solids [1]. In real materials, however, there are almost always disturbances, impurities, and irregularities that are either so small that they do not affect the physical properties or have to be actively addressed in the evaluation of the results. Concerning the latter case, disorder can often be a problem that makes the observation of interesting emergent phenomena difficult or destroys them altogether. For example, disorder can suppress the formation of new states of matter due to absent symmetries, or features that are actually sharp can only be seen rounded or smeared [2].

However, disorder does not always have to be a disadvantage that one tries to keep as low as possible, but can also be an opportunity to create new physics. A well known example can be found in the physics of semiconductors. Here dopant atoms are inserted into an almost perfect lattice structure by purpose to create local bound states with energies in between the energy gap of the semiconductor giving rise to a wide range of applications [1]. In 1977 the Nobel prize was awarded to P. W. Anderson for investigating the electronic properties of disordered systems. It was shown that in certain random lattices no diffusion takes place, but electrons are bound locally [3]. These disorder-induced localised particles can, for example, lead to a metal-insulator transition in weakly interacting many-electron systems [4]. In addition to the study of localisations in electronic systems and dynamical properties [5, 6] in disordered systems, the influence of disorder on phase transitions was also investigated [7–11]. It has been shown that disorder in some systems influences the universality class and can even change the order of the phase transition [12].

There are many different ways how disorder enters a system and how it can be described mathematically. This work focuses on quenched disorder, i.e., static disorder that does not change in the typical time scales of an experiment. In a theoretical model, impurities or vacancies can be described, for example, by a diluted model in which random grid points are taken out from the system [12]. Dislocations in the lattice structure can be described by introducing randomness in the strengths of the interactions between particles.

In this thesis the random transverse-field Ising model in one and two dimensions is simulated using the stochastic series expansion Monte Carlo method [13] and the critical behaviour at the phase transition is investigated. The disorder is introduced into the system by random bond and field strengths. The motivation of this work is to show that it is possible to simulate this type of random systems with our method. If the method turns out to be suitable, it can be applied analogously to a wide range of other models, e.g., geometrically frustrated systems, in the future.

This thesis is structured as follows: In Sec. 2, a brief introduction to phase transitions will be given. In particular, the critical behaviour at continuous quantum phase transitions, which are investigated in this thesis, will be discussed. The difference between quantum phase transitions in clean and disordered systems is elaborated on in Sec. 3. In Sec. 4, the quantum Monte Carlo method is described, which we use to simulate the finite temperature properties of the random transverse-field Ising model. It will also be explained how we can investigate zero temperature physics with a finite temperature simulation and which observables are measured. A brief description of the general procedure for inferring the critical behaviour of the infinite system by studying finite systems is given in Sec. 5. Then, connected to Sec. 3 different regimes of finite-size scaling behaviour of quantum systems with disorder and procedures to analyse them are presented. Finally, Sec. 6 contains the results for critical points and exponents of the random transverse-field Ising model in one and two dimensions. In Sec. 7, the thesis is summarised and an outlook is given.

2 Introduction to phase transitions

Phase transitions describe the abrupt transformation of a substance's state into another state, the properties of which clearly differ from the first state. Phase transitions are not only of great interest in statistical physics, but are fascinating phenomena that are also studied in, e.g., biology and chemistry. In the following chapter, phase transitions and their classification will be introduced by simple examples. The focus is on continuous phase transitions at zero temperature, also called continuous quantum phase transitions, and their critical behaviour. This chapter is based on the explanations in Refs. [14] and [12].

The best-known phase transitions in everyday life are the transitions from liquid water to steam and ice. Consider, for example, the melting of ice: Here, the continuous change in temperature caused by the addition of heat causes an abrupt change in the properties of the material. At the phase transition itself, a latent heat of fusion is required so that the solid ice changes into the liquid state. Transitions like this, where both phases coexist at the transition point, are called first-order phase transitions.

There are also phase transitions, where phases do not coexist and there is no latent heat. These are called second-order phase transitions, or continuous phase transitions. Both phases approach the same state driven by strong fluctuations at the point of the phase transition. The point of the phase transition, also called critical point, is dominated by the singular behaviour of physical quantities. A typical example of this would be the transition from a ferromagnet to a paramagnet by increasing the temperature, which causes the magnetic moments to fluctuate more and more until the absolute magnetisation vanishes at the critical point and the state becomes paramagnetic.

Landau theory provides a good framework to understand the mechanism behind continuous phase transitions: Here, the phases are distinguished by their underlying symmetry. The phase transition occurs at the point at which this symmetry is spontaneously broken. If we take up the example of the ferromagnet, it can be viewed in the simplest model as a composition of many freely alignable magnetic moments (spins). In the ferromagnetic phase, these point in the same direction leading to a finite macroscopic magnetisation in this direction, so that the state of the system is not invariant under rotation symmetry. In the paramagnetic phase the rotated

state looks the same macroscopically. In order to be able to quantify this symmetry breaking, an order parameter is defined that is linked to the broken symmetry. The order parameter is always zero in the symmetric, disordered phase and non-zero in the symmetry-broken, ordered phase. In our example, the total magnetisation of the ferromagnet would be a suitable order parameter.

2.1 Continuous quantum phase transitions

In addition to the classical or thermal phase transitions, which have just been described as examples, it is also possible to have phase transitions at vanishing temperature T. Transitions between two different quantum states at $T = 0$ are called quantum phase transitions. Such phenomena are driven by an external parameter such as a magnetic field h [12]. The reason for the continuous phase transition are no longer thermal but quantum fluctuations. Quantum fluctuations arise whens two or more terms in the Hamiltonian do not commute and therefore compete with each other. At the point of the phase transition, the symmetry of the Hamiltonian is spontaneously broken in the ground state and the properties of the system's ground state change [14].

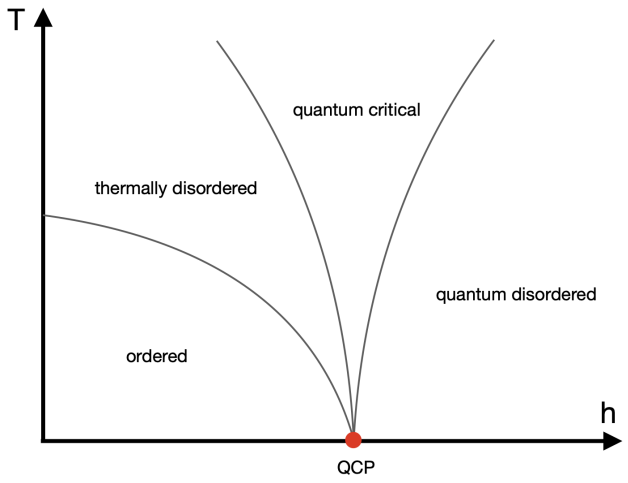

Figure 2.1: Illustration of the phase diagram as a function of temperature T and a control parameter h of a system with a line of thermal phase transitions and quantum-critical point.

Although quantum phase transitions are initially only defined at zero temperature, they still have an impact on the physics at finite temperatures. Starting from the quantum-critical point, a quantum-critical region is formed for $T > 0$ (see Fig. 2.1) [12]. Since it is not possible to cool a system down to zero temperature, the formation of the quantum-critical region is the only reason quantum phase transitions can be studied experimentally. Thus, the study of quantum phase transitions is not only interesting from a purely conceptual point, but also has a benefit for experiments and applications.

2.2 Critical exponents

Early on, experiments showed that a separate type of phase forms at the critical point. Since the second derivative of the free energy is not analytic at this point, this phase has the property that some observables, such as the correlation length, are singular [12]. The behaviour of these quantities near the critical point is described by power laws with critical exponents. The correlation length ξ behaves as

$$\xi \sim |r|^{-\nu} \ , \tag{2.1}$$

where ν is the corresponding critical exponent and r the control parameter defined as the reduced field strength

$$r = \frac{h - h_c}{h_c} \ . \tag{2.2}$$

The correlation time ξ_τ - the typical time scale of dynamics in the system - diverges as

$$\xi_\tau \sim |r|^{-z\nu} \tag{2.3}$$

at the critical point. Intuitively, the singular behaviour of correlation length and time means that close to a second order phase transition the system is correlated over large distances and any relaxation processes run very slowly. One also speaks of critical slowing down. z is the dynamical critical exponent connecting correlation length and correlation time close to the critical point

$$\xi_\tau \sim \xi^z \ . \tag{2.4}$$

In some systems with disorder, this relationship is no longer valid, which will be discussed in Sec. 3.2 and Sec. 5.1. The correlation time is directly connected to the typical energy scale

$$\Delta \sim |r|^{z\nu} \ , \tag{2.5}$$

which is in gapped systems usually associated with the energy gap between ground state and first excited state. The critical exponent β is related to the order parameter of the phase transition. In the case of a magnetic system this could correspond to the absolute magnetisation $|m|$, which vanishes as

$$|m| \sim |r|^{-\beta} \qquad r < 0 \tag{2.6}$$

at the critical field value h_c. Phase transitions are characterised by their set of critical exponents. Phase transitions in different systems are considered to be equivalent if they have the same critical exponents. The equivalence classes are called universality classes, which often contain potentially very different microscopic models. This is the case because the non-analytic properties of the phase transition do not depend on the microscopic details but are determined by basic properties such as the symmetries and the dimension of the system [14].

3 Phase transitions in disordered quantum systems

The influence of disorder on phase transitions has been studied for many decades. It turned out that randomness is able to change the order of a phase transition, change its universality class, or even make the transition disappear completely [12]. Since this thesis deals with the influence of disorder on continuous quantum phase transitions, the focus in this chapter lies on how disorder influences the behaviour of correlations and observables at the point of phase transition and in the vicinity of a continuous quantum phase transition. In Sec. 3.1 first the Harris criterion is introduced, which provides information about the stability of the critical point of a continuous phase transition with respect to the presence of disorder, followed by a description of the Griffiths phase in the vicinity of the critical point in Sec. 3.2. Both sections follow the explanations of T. Vojta's review on "Phases and phase transitions in disordered quantum systems" [12]. Then, the actual model we investigated in this work, the random transverse-field Ising model, is introduced in Sec. 3.3 and analytic results for the model in one dimension are presented.

3.1 The Harris criterion

In 1974, A. Harris [9] established a criterion for the stability of critical points with respect to disorder. It can be applied to both classical phase transitions driven by temperature and quantum phase transitions, e.g., driven by a transverse magnetic field h. The criterion is initially limited to short-range interactions, but can be generalised for long-range interactions [15]. The idea is the following: The infinite disordered system is divided into subsystems $\Omega^{(d)}$ with size ξ^d, where ξ is the correlation length and d is the dimension of the system. Now, one can imagine that each subsystem i has a different pseudo-critical point $h_c(i)$. The further one is away from the critical point, the smaller the correlation length and therefore the subsystems are. Due to finite-size effects, the finite-size critical point $h_c(i)$ is also farther away from the critical point h_c of the infinite system. Since in smaller systems the disorder is less averaged out, also the variation of the critical points Δh_c is increased. The distribution of critical points of the subsystems can be described by the central limit theorem since we average over many independent random variables $h_c(i)$. When approaching the point of phase transition the variation decays as

$$\Delta h_c(\xi(h)) \sim \xi^{-d/2} \ . \tag{3.1}$$

We further know that the correlation length scales as

$$\xi \sim |h - h_c|^{-\nu} \tag{3.2}$$

in the vicinity of the critical point (see Sec. 2.2). We can now distinguish two cases: In the first case, when

$$\lim_{h \to h_c} \frac{\Delta h_c}{|h - h_c|} \to 0 \quad \Rightarrow \quad d\nu > 2 \ , \tag{3.3}$$

the Harris criterion is fulfilled. This means that at the phase transition, when the correlation length and thus the system size of the subsystems diverges, the variations Δh_c in the subsystems become less and less important and the system looks less and less disordered. The system is stable at the critical point against the disorder and the universality class remains the same [12]. In systems that fulfil the Harris criterion, one also speaks of self-averaging, since observables in the infinite system no longer depend on the exact configuration of the disorder, but have the same value for every realisation of an infinite system [12]. In the second case, when

$$\lim_{h \to h_c} \frac{\Delta h_c}{|h - h_c|} \to \infty \quad \Rightarrow \quad d\nu < 2 \ , \tag{3.4}$$

the Harris criterion is not fulfilled. This means that at the critical point there are still variations in the distribution of pseudo-critical points and the critical point is not stable with respect to disorder. In this case, the property of self-averaging of observables is not fulfilled either [12]. In general, the phase transition will change its universality class [16].

The Harris criterion is interesting for us because it predicts which problems we could expect when simulating disordered quantum systems. The random transverse-field Ising model (see Sec. 3.3) in one and two dimensions that we want to simulate does not fulfil the Harris criterion, which means that, on the one hand, we expect modified critical exponents compared to the clean system and, on the other hand, the systems will not be self-averaging. This influences our simulation in such a way that, even for large finite systems, we still have to average over many disorder realisations in order to get good mean values.

3.2 Rare regions and Griffiths singularities

In disordered systems, singular behaviour is not restricted to the critical point but can also appear in its vicinity. These phenomena are known as Griffiths singularities [7, 8]. They are caused by so-called rare regions. Rare regions are finite areas that show a very unusual disorder configuration, e.g., when a finite cluster is completely separated from the rest of the lattice in a diluted system or when all bonds in a region have an extreme value in a random bond strength model. Rare regions display their own critical behaviour, which does not occur at the same point as the

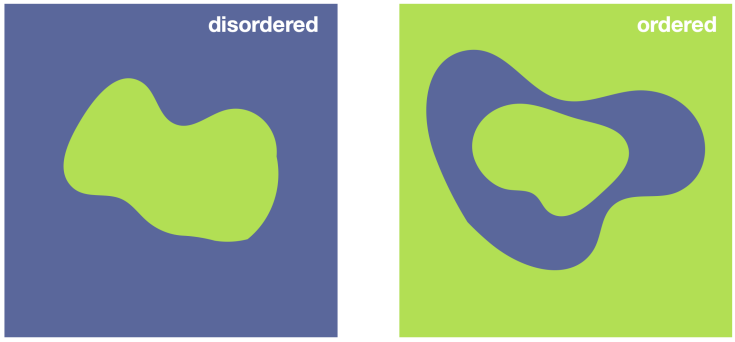

Figure 3.1: Visualisation of rare regions in the disordered (left) and ordered (right) phase.

global phase transition due to their individual properties and finite-size effects. The area in which they occur is called the Griffiths phase. They can be found both in the disordered and ordered phase. In the disordered phase, rare regions are given by strongly correlated regions that are ordered even if the macroscopic state of the system is disordered (see Fig. 3.1 on the left). The probability of finding a rare region of size L_R is exponentially small

$$P(L_R) \sim e^{-\alpha L_R^d} \ , \tag{3.5}$$

where α depends on the kind of disorder and the dimension d of the system [17]. In the ordered phase, the rare regions also consist of strongly-correlated, ordered regions. In this case, however, they are separated from the macroscopic ordered state by another disordered region such that they are not connected to the macroscopic ordered state (see Fig. 3.1 on the right) and can therefore fluctuate independently. The probability of finding rare regions of a certain size in the ordered phase is smaller than in the disordered phase due to the additional disordered phase in between [17]. For $d > 1$, the probability is given by

$$P(L_R) \sim e^{-\alpha L_R^{d^2}} \ . \tag{3.6}$$

Although the number of rare regions is exponentially suppressed, their contribution to observables is still $O(1)$. The reason for this is that the energy gap Δ in the finite regions is exponentially small and the relaxation time of the states τ_R is therefore exponentially large [17]

$$\Delta \sim e^{-\sigma L_R^d} \qquad\qquad \tau_R \sim e^{\sigma L_R^d} \ . \tag{3.7}$$

If one tries to measure the contribution of the Griffiths singularities close to the phase transition, it is striking that in classical systems there is hardly any contribution to be found in observables such as magnetisation or susceptibility [12]. In the case of quantum phase transitions, on the other hand, the influence can be far greater. Furthermore, due to the larger number of rare regions in the disordered phase, the

contribution of the Griffiths singularities is greater in the disordered phase than in the ordered phase.

To obtain averaged quantities, we have to calculate a large number of disorder configurations. Some of them will also look very atypical, especially for small system sizes. From the discussion about rare regions in infinite systems we can learn that these few rare configurations are important for the correct calculation of our mean values of observables and therefore should not be neglected. Furthermore, very small energy gaps Δ in the systems mean that we have to go to very low temperatures in the finite temperature Monte Carlo simulations to simulate the ground state (see Sec. 4.5. Moreover, we can detect the influence of the Griffiths singularities on dynamical scaling directly in the paramagnetic phase (see Sec. 6.3).

3.3 Random transverse-field Ising model

Transverse-field Ising model

The Hamiltonian of the transverse-field Ising model (TFIM) [18, 19] is given by an Ising term connecting spin-1/2 degrees of freedom located at neighbouring lattice sites i and j in z-direction and a magnetic field term in x-direction acting on each individual spin-1/2 degree of freedom

$$H = -J \sum_{\langle i,j \rangle} \sigma_i^z \sigma_j^z - h \sum_i \sigma_i^x \ . \tag{3.8}$$

Looking at the model in the z-basis, the σ^z operators of the Ising term preferably align two neighbouring spins i and j in the same direction for $J > 0$ and in opposite direction for $J < 0$. The field term is flipping spins with σ^x operators. Since σ^z and σ^x do not commute, the TFIM is a quantum model.

In the low-field limit $h = 0$ for ferromagnetic couplings $J > 0$, the ground state is either the state where all spins are pointing up or where all spins are pointing down. In the antiferromagnetic case $J < 0$ for bipartite lattices, i.e., lattices where every closed loop on the lattice consists of an even number of bonds, the situation is similar. The two degenerate ground states are $|\Uparrow\Downarrow\Uparrow\ ...\rangle$ and $|\Downarrow\Uparrow\Downarrow\ ...\rangle$. For non-bipartite lattices, e.g., the two-dimensional triangular lattice, the situation is different: Since it is not possible that all neighbouring spins are energetically favourable aligned, the ground state is highly degenerate due to geometric frustration. In the ground state of the high-field limit $h = \infty$ all spins are aligned in the direction of the field. Excitations can be created by flipping spins to the opposite direction.

For antiferromagnetic bipartite and ferromagnetic lattices, the ordered phase ($h \ll J$) and the disordered phase ($h \gg J$) can be distinguished from each other by a $\mathbb{Z}_2$-symmetry. For $h < h_c$, the ground state's symmetry is spontaneously broken.

The phase transition is known to be within the $(d+1)$D-Ising universality class [14], where d is the dimension of the system. In the case of non-bipartite lattices and antiferromagnetic interactions, the situation is more difficult and strongly depends on the lattice structure [20–23]. A finite transverse field h leads to the degeneracy at $h = 0$ being broken up. In the case of the triangular lattice, the system transitions into a clock ordered phase, one speaks of order by disorder [20–22] (here disorder denotes the quantum fluctuations induced by the transverse field, not randomness). For higher fields h there is a phase transition from the ordered phase to the polarised high-field phase with universality class 3DXY [21]. In the case of the frustrated Kagome lattice, the system goes directly into the polarised phase, which is called disorder by disorder [23].

Random transverse-field Ising model

In the random transverse-field Ising model (RTFIM)

$$H = -\sum_{\langle i,j \rangle} J_{ij}\sigma_i^z\sigma_j^z - \sum_i h_i\sigma_i^x \tag{3.9}$$

the bond strengths J_{ij} and field strengths h_i are not equal for every bond, but are drawn from probability distributions (see Fig. 3.2)

$$J_{ij} \in P(X) \qquad h_i \in P'(X)\ . \tag{3.10}$$

Therefore, some major things change compared to the clean system. First of all, there is no translational symmetry, such that the problem can not be simplified by performing a Fourier transformation. In addition, especially for finite systems, the value of observables is not only affected by finite-size effects, but also by the specific disorder configuration $\{J_{ij}, h_i\}$ on the lattice.

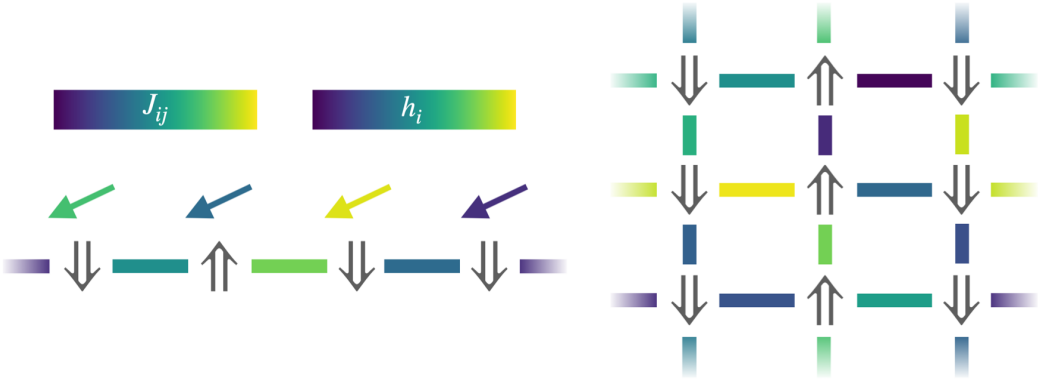

Figure 3.2: Visualisation of the RTFIM in one dimension with disorder in bond and field strengths (left) and in two dimension on the square lattice with disorder in the bond strengths only. The strength of the bonds J_{ij} (connections between spins) and fields h_i (arrows above spins) is indicated by their colour.

Analogous to the clean system, a distinction must be made between ferromagnetic and antiferromagnetic systems. In the case of ferromagnetic systems, the phase diagram looks qualitatively very similar to that of the clean system. For small fields $\langle h_i \rangle \ll \langle J_{ij} \rangle$ (with moderate disorder) the system is in an ordered ground state. For large fields, the system then transitions to the polarised phase. A suitable order parameter to describe the symmetry breaking is the squared magnetisation

$$m^2 = \frac{1}{N^2} \left(\sum_i \sigma_i^z \right)^2 . \tag{3.11}$$

However, as soon as the Harris criterion is not fulfilled, the criticality of the phase transition will change. The same behaviour as for the ferromagnetic systems is expected for antiferromagnetic systems on bipartite lattices. On non-bipartite lattices it is unknown how the disorder affects the frustrated ground state and the resulting phases. This could be the focus of future projects. In this thesis only ferromagnetic systems are addressed. The simplest system is the one-dimensional RTFIM, which will be discussed in the following subsection.

3.3.1 Analytic results for the chain

For the random transverse-field Ising chain (RTFIC) the position of the critical point for any finite disorder realisation can be calculated analytically up to a small contribution of a neglected boundary term. This calculation was first carried out by Pfeuty in 1979 [10] using a Jordan Wigner transformation and will be presented in this section. The Hamiltonian of the RTFIC with N spins simplifies to

$$H = -\sum_{i=1}^{N} h_i \sigma_i^x + \sum_{i=1}^{N} J_i \sigma_i^z \sigma_{i+1}^z , \tag{3.12}$$

with periodic boundary conditions

$$\sigma_{N+1}^{x/z} = \sigma_1^{x/z} . \tag{3.13}$$

In a first step, the coordinate system is rotated in the xz-plane ($\sigma^x \to -\sigma^z$ and $\sigma^z \to \sigma^x$) such that

$$H = \sum_{i=1}^{N} h_i \sigma_i^z + \sum_{i=1}^{N} J_i \sigma_i^x \sigma_{i+1}^x . \tag{3.14}$$

In the next step, the Pauli matrices are expressed by creation and annihilation operators fulfilling hardcore-bosonic properties

$$\sigma_i^z = 1 - 2 b_i^\dagger b_i \qquad \sigma_i^x = b_i^\dagger + b_i \tag{3.15}$$

$$[b_i^\dagger, b_j] = \delta_{ij} \qquad [b_i, b_j] = [b_i^\dagger, b_j^\dagger] = 0 . \tag{3.16}$$

The Hamiltonian can then be written as

$$H = -\sum_{i=1}^{N} h_i \left(2b_i^\dagger b_i - 1\right) + \sum_{i=1}^{N} J_i \left(b_i^\dagger b_{i+1}^\dagger + b_i^\dagger b_{i+1} + h.c.\right) \ . \tag{3.17}$$

Using a Jordan Wigner transformation, the bosonic operators can be mapped to fermionic operators. This method, followed by a Fourier transformation, is also used analogously to solve the clean transverse-field Ising chain exactly [24]. The transformation is given by

$$b_i^\dagger = \exp\left(-\mathrm{i}\pi \sum_{k=1}^{i-1} c_k^\dagger c_k\right) c_i^\dagger \tag{3.18}$$

$$b_i = \exp\left(\mathrm{i}\pi \sum_{k=1}^{i-1} c_k^\dagger c_k\right) c_i \tag{3.19}$$

The fermionic creation and annihilation operators $c_i^\dagger, c_i$ satisfy anti-commutation relations

$$\{c_i^\dagger, c_j\} = \delta_{ij} \qquad \{c_i, c_j\} = \{c_i^\dagger, c_j^\dagger\} = 0 \tag{3.20}$$

and are inserted into the Hamiltonian. The field term remains unchanged in its form since the particle-counting operator in the fermionic picture is equal to the particle-counting operator in the hardcore-bosonic picture

$$n_i := b_i^\dagger b_i = c_i^\dagger c_i \ . \tag{3.21}$$

Making use of the identity $\exp(\pm\mathrm{i}2\pi n) = 1$ with $n \in \mathbb{N}$, one finds

$$\begin{aligned} H = &-\sum_{i=1}^{N} h_i \left(2c_i^\dagger c_i - 1\right) - \sum_{i=1}^{N-1} J_i \Big[c_i^\dagger c_{i+1}^\dagger \exp\left(-\mathrm{i}\pi n_i\right) + c_i^\dagger c_{i+1} \exp\left(\mathrm{i}\pi n_i\right) \\ &+ c_i c_{i+1} \exp\left(\mathrm{i}\pi n_i\right) + c_i c_{i+1}^\dagger \exp\left(-\mathrm{i}\pi n_i\right)\Big] \\ &- J_N \left[c_N^\dagger \exp\left(-\mathrm{i}\pi \sum_{k=1}^{N-1} n_k\right) c_1^\dagger + c_N^\dagger \exp\left(-\mathrm{i}\pi \sum_{k=1}^{N-1} n_k\right) c_1 \right. \\ &\left. + c_N \exp\left(\mathrm{i}\pi \sum_{k=1}^{N-1} n_k\right) c_1 + c_N \exp\left(\mathrm{i}\pi \sum_{k=1}^{N-1} n_k\right) c_1^\dagger\right] \ , \end{aligned} \tag{3.22}$$

where the periodic boundary needs special treatment. The phase factors $\exp\left(\pm\mathrm{i}\pi n_i\right)$ can be evaluated in the following way: If an operator c_i is in front of the phase factor, there has to be a fermionic quasi-particle at position i because otherwise the state is destroyed. Therefore, the phase factor is equal to $\exp\left(\pm\mathrm{i}\pi \cdot 1\right) = -1$. In

the case of an operator $c_i^\dagger$ being in front of the phase factor, the opposite is true: $\exp(\pm \mathrm{i}\pi \cdot 0) = 1$. Similar arguments for the boundary term lead to

$$\begin{aligned} H = &- \sum_{i=1}^{N} h_i \left(2c_i^\dagger c_i - 1\right) - \sum_{i=1}^{N-1} J_i \left[c_i^\dagger c_{i+1}^\dagger + c_i^\dagger c_{i+1} - c_i c_{i+1} - c_i c_{i+1}^\dagger\right] \\ &- J_N \left[c_N^\dagger \exp\left(-\mathrm{i}\pi \sum_{k=1}^{N} n_k\right) c_1^\dagger + c_N^\dagger \exp\left(-\mathrm{i}\pi \sum_{k=1}^{N} n_k\right) c_1 \right. \\ &\left. - c_N \exp\left(\mathrm{i}\pi \sum_{k=1}^{N} n_k\right) c_1 - c_N \exp\left(\mathrm{i}\pi \sum_{k=1}^{N} n_k\right) c_1^\dagger\right] . \end{aligned} \tag{3.23}$$

The phase factors in the boundary term can be permuted with the creation and annihilation operators taking care of the anti-commutation relations. The missing terms $\sim J_N$ in the second sum can be added from the boundary term

$$\begin{aligned} H = &- \sum_{i=1}^{N} h_i \left(2c_i^\dagger c_i - 1\right) - \sum_{i=1}^{N} J_i \left[c_i^\dagger c_{i+1}^\dagger + c_i^\dagger c_{i+1} - c_i c_{i+1} - c_i c_{i+1}^\dagger\right] \\ &- J_N \left[c_N^\dagger c_1^\dagger + c_N^\dagger c_1 - c_N c_1 - c_N c_1^\dagger\right] \left(\exp\left(\mathrm{i}\pi \sum_{k=1}^{N} n_k\right) + 1\right) . \end{aligned} \tag{3.24}$$

At this point, the boundary term is neglected. Since it does only contain a small local contribution, this term should vanish for sufficiently large system sizes. The remaining Hamiltonian can be brought into a quadratic form

$$H' := -\frac{1}{2} H = \sum_{ij} c_i^\dagger A_{ij} c_j + \frac{1}{2} \left(c_i^\dagger B_{ij} c_j^\dagger + h.c.\right) , \tag{3.25}$$

with the matrices A and B

$$A = \begin{pmatrix} h_1 & J_1/2 & & & & J_N/2 \\ J_1/2 & \ddots & \ddots & & & \\ & \ddots & \ddots & \ddots & 0 & \\ & 0 & \ddots & \ddots & \ddots & \\ & & & \ddots & \ddots & J_{N-1}/2 \\ J_N/2 & & & & J_{N-1}/2 & h_N \end{pmatrix} \tag{3.26}$$

$$B = \begin{pmatrix} 0 & J_1/2 & & & & -J_N/2 \\ -J_1/2 & & \ddots & & & \\ & \ddots & & \ddots & 0 & \\ & 0 & \ddots & & \ddots & \\ & & & \ddots & & J_{N-1}/2 \\ J_N/2 & & & & -J_{N-1}/2 & 0 \end{pmatrix} . \tag{3.27}$$

Using a linear ansatz for the eigenfunctions of the Hamiltonian

$$\eta_k = \sum_i g_{ki} c_i + h_{ki} c_i^\dagger \tag{3.28}$$

we can rewrite the Hamiltonian as

$$H' = \sum_k \Lambda_k \eta_k^\dagger \eta_k \tag{3.29}$$

satisfying

$$[\eta_k, H'] = \Lambda_k \eta_k \ . \tag{3.30}$$

We can now plug in the former definition of the Hamiltonian from Eq. 3.25 into Eq. 3.30 to obtain a relation between g, h and the matrices A and B. Comparing the coefficients in front of the operators c_i and $c_i^\dagger$ leads to the relations

$$\Lambda_k g_{ki} = \sum_j g_{kj} A_{ji} - h_{kj} B_{ji} \quad \text{and} \quad \Lambda_k h_{ki} = \sum_j g_{kj} B_{ji} - h_{kj} A_{ji} \ . \tag{3.31}$$

Introducing linear combinations of the coefficients $\phi_{ki} = g_{ki} + h_{ki}$ and $\psi_{ki} = g_{ki} - h_{ki}$, Eq. 3.31 can be decoupled to

$$\phi_k (A-B)(A+B) = \Lambda_k^2 \phi_k \qquad \psi_k (A+B)(A-B) = \Lambda_k^2 \psi_k \ . \tag{3.32}$$

The solution of this secular equation is given by

$$\det\left((A+B)(A-B) - \Lambda_k^2 \mathbb{1}\right) = 0 \ . \tag{3.33}$$

Since we are interested in the critical point, we search for the point where the excitation energy Λ_k is equal to zero. Actually, one would expect that the energy gap Λ_k does not close completely at the pseudo-critical point of a finite system but remains finite (see Sec. 5). In this calculation, this is a remnant of the neglected boundary term. We can evaluate the determinant for $\Lambda_k = 0$ using a Laplace expansion of $(A-B) = (A+B)^T$

$$\det(A-B) = \det \begin{pmatrix} h_1 & & & & & J_N \\ J_1 & \ddots & & & & \\ & \ddots & \ddots & 0 & & \\ & 0 & \ddots & \ddots & & \\ & & & \ddots & \ddots & \\ & & & & J_{N-1} & h_N \end{pmatrix} = \prod_i^N h_i - \prod_i^N J_i \ . \tag{3.34}$$

This gives us the relation

$$\prod_i h_i = \prod_i J_i \tag{3.35}$$

between the strengths of the Ising bonds J_i and the field strengths h_i at the critical point. In the case with no disorder in the field strengths h, the equation can be used to determine the sample-dependent critical point $\widetilde{h}_c$ only by knowing the J_i used in the given configuration

$$\widetilde{h}_c = \left(\prod_i^N J_i \right)^{1/N} . \tag{3.36}$$

In the thermodynamic limit, the contribution of the neglected boundary term should vanish and therefore

$$\lim_{N \to \infty} \widetilde{h}_c \to h_c \ . \tag{3.37}$$

Eq. 3.36 is important because it allows us to test our numerical methods for determining the pseudo-critical point of a disorder configuration. As can be seen in Sec. 6.1, we can even see the influence of the boundary term, which becomes smaller and smaller with increasing system sizes.

4 Stochastic series expansion quantum Monte Carlo

In this chapter we first review the basic concept of Monte Carlo integration methods and then introduce the Stochastic Series Expansion in the second part, which is the quantum Monte Carlo method used to simulate the RTFIM in this thesis.

4.1 Introduction to Monte Carlo methods

Monte Carlo integration is an efficient way to calculate high-dimensional integrals. As the name suggests, randomness is used for this purpose. In contrast to conventional integration methods, where a fixed grid of points in space is used to determine the value of the integral, Monte Carlo methods use random points in configuration space [25]. This has a decisive advantage: Suppose you want to calculate the value of an integral of the form

$$I = \int_{\Omega} f(\vec{x})\, d\vec{x}\ , \tag{4.1}$$

where Ω is an arbitrary configuration space of dimension d. For M random points $\vec{x}_i$ with corresponding value $f(\vec{x}_i)$, the estimator for the value of the integral

$$\langle I \rangle = \frac{1}{M} \sum_{i=1}^{M} f(\vec{x}_i) \tag{4.2}$$

can be assumed to be a Gaussian function according to the central limit theorem. The estimator's standard deviation

$$\sigma^2 = \frac{1}{M} \left(\langle I^2 \rangle - \langle I \rangle^2 \right) \tag{4.3}$$

scales with $1/M$. Thus, the error of the estimator scales independently of the dimension d with $1/\sqrt{M}$. In contrast, the accuracy of conventional methods for numerical integration always scales with the dimension of the configuration space and therefore performs very poorly for high-dimensional integrals [25].

An application where this property of the Monte Carlo method is important is the calculation of expectation values of observables $\mathcal{O}$ in statistical physics

$$\langle \mathcal{O} \rangle = \int_{\Omega} \mathcal{O}(\vec{x}, \vec{p})\, P(\vec{x}, \vec{p})\, d\vec{x}\, d\vec{p}\ , \tag{4.4}$$

where $P(\vec{x}, \vec{p})$ is the Boltzmann distribution. In three-dimensional space with N particles in the system located at position $\vec{x}$ with momentum $\vec{p}$, the configuration space has dimension $d = 6N$ [26]. With typically large numbers of particles, the advantage of Monte Carlo methods over conventional sampling methods increases drastically.

Markov chain Monte Carlo

The motivation for the following method is that often a non-normalised probability distribution $\tilde{p}$ is known and samples and expectation values are supposed to be drawn from it. In the general case, it is not possible to calculate the normalisation constant and thus get the desired normalised distribution p. Another problem is that direct sampling of arbitrary probability distributions is often not feasible. Markov chains can be used to generate random samples of a configuration space distributed according to an arbitrary probability distribution. The following explanations on Markov chain Monte Carlo and the Metropolis Hastings algorithm are based on Ref. [27].

Markov processes are stochastic processes without memory. This means that the probability for performing a move to the next state only depends on the current state and not any previous states. The probability to go from state x to x' in (finite) Markov chains is given by the transition element

$$T(x'|x) = P(x \to x') \quad \text{with} \quad T(x'|x) \geq 0, \quad \sum_{x'} T(x'|x) = 1 \ \forall x \ . \tag{4.5}$$

The chain starts with an initial probability distribution $p^{(0)}$ which is updated in each step. The probability distribution at step k

$$p^{(k)}(x') = \sum_{x} p^{(k-1)}(x)\, T(x'|x) \tag{4.6}$$

only depends on the probability distribution of the previous step. A probability distribution is called a stationary distribution π if it satisfies the global balance condition

$$\pi(x') = \sum_{x} \pi(x)\, T(x'|x) \ . \tag{4.7}$$

The goal is to choose the transition element T such that π corresponds to the desired distribution p. A way to ensure the existence of an stationary distribution is to fulfil the condition of irreducibility. This means that every state can be reached from every other state. Moreover the expected return time, i.e. the mean time until a state returns to the same state, should be finite [27]. In addition, we want the distribution $\pi = p$ to which the Markov chain converges to be unique. To fulfil this, the process has to be aperiodic, i.e., the state should not return to the same state at regular intervals. In contrast to other importance or rejection sampling procedures, the advantage of Markov chain sampling is that it performs very well even in high-dimensional configuration spaces [27].

Metropolis Hastings algorithm

The Metropolis Hastings algorithm is a Markov chain algorithm that satisfies the condition of detailed balance

$$p(x)\,T(x'|x) = p(x')\,T(x|x')\ , \tag{4.8}$$

which implies global balance. Based on this condition, the following steps can be derived in order to draw from the desired distribution p using a known, normalized probability distribution $q(x'|x)$ and the known distribution $\tilde{p} \sim p$:

1. Propose move to x' with probability $q(x'|x^{(k-1)})$.
2. Accept move with probability $a = \min\left(1,\ \frac{\tilde{p}(x')\,q(x^{(k-1)}|x')}{\tilde{p}(x^{(k-1)})\,q(x'|x^{(k-1)})}\right)$.
3. If accepted, set $x^{(k)} = x'$. Otherwise set $x^{(k)} = x^{(k-1)}$.

The beginning of the sampling is biased since the initial distribution might not be in a dominant part of the configuration space. To circumvent artefacts of this "burn-in" in the results of the sampling, often the first samples are thrown away. Furthermore the efficiency is highly dependent on the choice of the proposal distribution q.

4.2 Stochastic series expansion

The stochastic series expansion (SSE) approach is a quantum Monte Carlo method based on a high-temperature expansion of the partition function to simulate finite spin systems. It has been developed by A. Sandvik [13, 28] and is a generalisation of Handscomb's method [29]. In contrast to Handscomb's method it is applicable to a wide range of models. The following description of the method is limited to the application to the RTFIM. More general descriptions and implementation details can be found in Refs. [26, 30–32].

Before we turn to the actual quantum Monte Carlo algorithm, we must first rewrite the Hamiltonian into a suitable form. The Hamiltonian of the RTFIM with N sites

$$H = -\sum_{\langle ij\rangle} J_{ij}\sigma_i^z\sigma_j^z - \sum_{i}^{N} h_i\sigma_i^x\ , \tag{4.9}$$

consists of an Ising term that is diagonal in the z-basis

$$\{|\alpha\rangle\} = \{|\sigma_1^z, ...\sigma_N^z\rangle\} \tag{4.10}$$

and a field term that flips spins in the z-basis and is therefore not diagonal. It can be decomposed into elementary operators

$$H_{0,0} = \mathbb{1} \qquad H_{i,0} = h_i\,(\sigma_i^+ + \sigma_i^-) \tag{4.11}$$

$$H_{i,i} = h_i \qquad H_{i,j} = |J_{ij}| - J_{ij}\,\sigma_i^z\sigma_j^z \tag{4.12}$$

with $i, j \in \{1, ..., N\}$, which are chosen such that their amplitudes are non-negative regarding the chosen z-basis. Furthermore, it fulfils the non-branching rule

$$H_{a,b}|\beta\rangle \sim |\gamma\rangle \qquad a, b \in \{0, \ldots, N\} \tag{4.13}$$

for all $|\beta\rangle, |\gamma\rangle \in \{|\alpha\rangle\}$, which basically means that no superpositions of states are allowed to arise when acting with $H_{a,b}$ on basis states. The Hamiltonian can then be written as the sum of these operators

$$H = -\sum_{i=1}^{N}\sum_{j=0}^{N} H_{i,j} + c \;, \tag{4.14}$$

where $H_{0,0}$ is introduced for implementation reasons only and is not part of the original Hamiltonian.

The first step of the SSE approach is the expansion of the partition function in powers of βH. The trace over the operators is executed in the orthogonal basis $\{|\alpha\rangle\}$. The decomposed Hamiltonian from Eq. 4.14 is inserted into the partition function

$$Z = \mathrm{Tr}(e^{-\beta H}) = \sum_{\{|\alpha\rangle\}}\sum_{n=0}^{\infty} \frac{(-\beta)^n}{n!} \langle\alpha| H^n |\alpha\rangle \tag{4.15}$$

$$= \sum_{\{|\alpha\rangle\}}\sum_{n=0}^{\infty} \frac{\beta^n}{n!} \langle\alpha| \Big(\sum_{i=1}^{N}\sum_{j=0}^{N} H_{i,j}\Big)^n |\alpha\rangle \;. \tag{4.16}$$

Using the binomial expansion of the power of the decomposed Hamiltonian the result is a sum of products of elementary operators with length n. These products of operators with length n are called sequences S_n in the following. Instead of summing over all combinations of operators, it is now summed over all possible sequences S_n, where each element of a sequence at position l corresponds to an index pair $[i(l), j(l)]$ that can be associated with an operator $H_{i(l),j(l)}$. The partition function can then be written as

$$Z = \sum_{\{|\alpha\rangle\}}\sum_{n=0}^{\infty}\sum_{S_n} \frac{\beta^n}{n!} \langle\alpha| \prod_{l=1}^{n} H_{i(l),j(l)} |\alpha\rangle \;. \tag{4.17}$$

It turns out that sequences longer than $L \sim \beta N$ contribute only exponentially little to the sum [26, 30]. It is advantageous for computer simulations if all sequences are of the same finite length, which is why the fixed length scheme is introduced. All sequences are truncated at a certain sufficiently long length L, which is determined iteratively during the simulation (see Sec. 4.5) such that there is no truncation error. Trivial operators $H_{0,0}$ are added to sequences smaller than L so that all have the same length. The number of non-trivial operators in the sequence is denoted by n_{S_L} in the following. Since the $L - n_{S_L}$ inserted trivial operators can be at any position in the

sequence, equivalent configurations occur more than once in the partition function if we sum over all possible sequences with length L including trivial operators. To preserve the weights of the original configuration-space elements we have to divide by a combinatorical factor to compensate overcounting:

$$Z \approx \sum_{\{|\alpha\rangle\}} \sum_{S_L} \frac{\beta^n}{n_{S_L}!} \frac{n_{S_L}!(L-n_{S_L}!)}{L!} \langle\alpha| \prod_{l=1}^{L} H_{i(l),j(l)} |\alpha\rangle \ . \tag{4.18}$$

Having a closer look at the matrix elements, inserting $\mathbb{1} = \sum_k |\alpha^{(k)}\rangle\langle\alpha^{(k)}|$ between the single operators, leads to a chain of matrix elements

$$\langle\alpha| \prod_{l=1}^{L} H_{i(l),j(l)} |\alpha\rangle = \langle\alpha^{(L)}| H_{i(L),j(L)} |\alpha^{(L-1)}\rangle\langle\alpha^{(L-1)}| \ldots |\alpha^{(1)}\rangle\langle\alpha^{(1)}| H_{i(1),j(1)} |\alpha^{(0)}\rangle \tag{4.19}$$

with the periodic boundary condition resulting from the trace

$$|\alpha^{(0)}\rangle = |\alpha^{(L)}\rangle = |\alpha\rangle \ . \tag{4.20}$$

At this point, the need for the non-branching property becomes apparent. With this extra dimension of propagation, often called imaginary time, the configuration space we sample with Monte Carlo integration becomes

$$\Omega = \{|\alpha\rangle\} \times \{S_L\} \ . \tag{4.21}$$

A single configuration of Ω can be visualized as shown in Fig. 4.1. The partition function can now be defined as a sum of weights of the states in the configuration space Ω

$$Z = \sum_{\omega\in\Omega} w(\beta,\omega) \tag{4.22}$$

$$w(\beta,\omega) = \frac{\beta^n (L-n_{S_L})!}{L!} \langle\alpha| \prod_{l=1}^{L} H_{i(l),j(l)} |\alpha\rangle \ . \tag{4.23}$$

This is a good starting point for an efficient simulation since it suffices to only successively act with operators on one or two spins to calculate the weights of a configuration. Furthermore, one only has to save the initial state of the system $|\alpha\rangle$, since any other intermediate state in imaginary-time direction

$$|\alpha^{(k)}\rangle = \prod_{l=1}^{k} H_{i(l),j(l)} |\alpha\rangle \tag{4.24}$$

can simply be reconstructed from the sequence of operators.

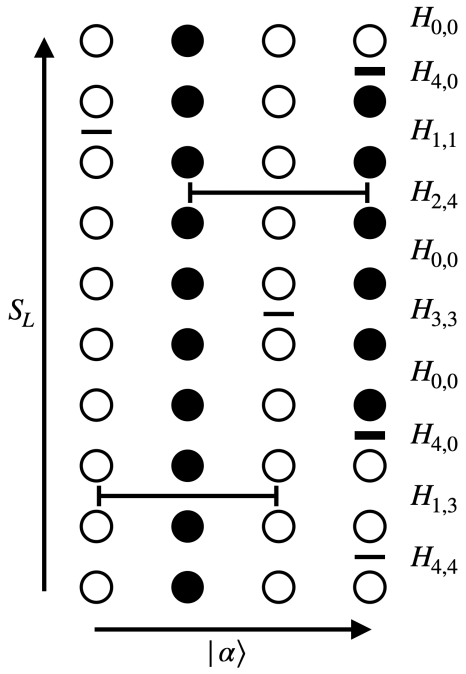

Figure 4.1: Visualization of a typical sequence with length $L = 10$ in a $N = 4$ ferromagnetic spin system. Filled circles correspond to the spin-up state, unfilled circles to the spin-down state. Constant operators $H_{i,i}$ are represented by thin lines, field operators $H_{i,0}$ by thick lines. If an Ising operator $H_{i,j}$ acts on two spins, they are connected by a large line.

4.3 Update of configurations

In order to sample the configuration space of a system, we first need the information about the lattice structure of the system, i.e. bondfiles, that tell us, which spins are connected via bonds in the lattice structure, and the temperature $T \sim 1/\beta$ at which we want to simulate the system. The simulation starts with an initial configuration Ω^0 that is constantly updated. During these updates, the operators in the sequence are iteratively exchanged and both the propagated states and the initial states can change [13]. This changes the weight $w(\beta, \omega)$ and the value of observables measured during the updates. Details concerning the measurement of observables can be found in Sec. 4.4. An important condition for the updates is that the new configuration after the update does not have zero weight [30]. This happens, for example, when the periodic boundary conditions are not fulfilled in imaginary time or the amplitude of an operator acting on the propagated state is zero. A full update, also called Monte Carlo sweep, is given by successively performing a diagonal update and an off-diagonal update. In Sec. 4.3.1, the diagonal update, which is based on the Metropolis-Hastings algorithm and changes only the weight $w(\beta, \omega)$, is presented. Moreover, we introduce an efficient way to draw random numbers. Off-diagonal updates are presented in Sec. 4.3.2, which keep $w(\beta, \omega)$ the same, but change the state $|\alpha\rangle$.

4.3.1 Diagonal update

In the diagonal update, operators are replaced that are diagonal in the z-basis. In the case of the transverse-field Ising model, these are the constant operators $H_{i,i}$, Ising operators $H_{i,j}$ and trivial operators $H_{0,0}$. Diagonal operators can not change the state $|\alpha\rangle$ of the system, but can change the weight of the configuration if a trivial operator is replaced by a non-trivial one and vice versa. During the diagonal

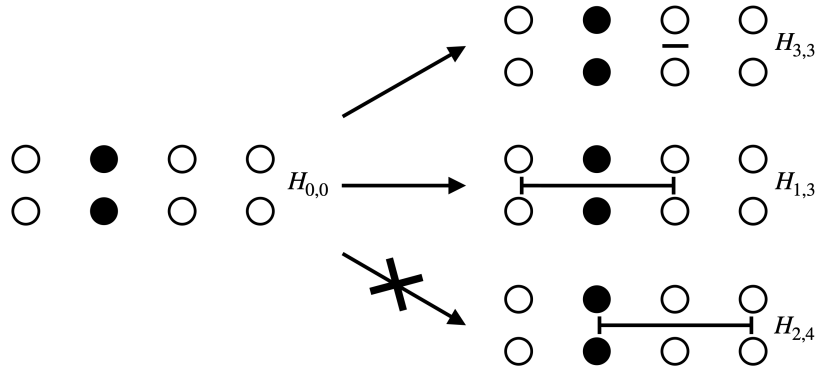

Figure 4.2: Insertion of operators during the diagonal update in a ferromagnetic spin system. Constant operators may be inserted at any position (top). Ising operators can only be inserted if both spins they act on have the same state (middle) and not if they have different states (bottom).

update, the sequence is successively traversed and at each position k of the sequence a trivial operator is exchanged by a non-trivial operator with a certain acceptance probability and vice versa.

The probability of an operator being inserted is determined using the Metropolis-Hastings algorithm described in Sec. 4.1. First, the normalised proposal probability of replacing a trivial operator by a non-trivial operator is chosen by the eigenvalues of the respective operators

$$q(H_{0,0} \to H_{i,j}) = \frac{M_{ij}}{\sum_i h_i + 2\sum_{i\neq j} |J_{ij}|} \tag{4.25}$$

$$M_{ij} = \begin{cases} 2|J_{ij}| \text{ or } 0 & i \neq j \\ h_i & i = j \end{cases} . \tag{4.26}$$

For the case $i \neq j$ one must be aware, that the eigenvalue of $H_{i,j}$ can also be zero. This must be checked in the algorithm before inserting the operator. In this case, the operator is not inserted since otherwise the weight of the entire configuration would be zero. The opposite operation of exchanging a non-trivial operator by a trivial operator is proposed with probability one

$$q(H_{i,j} \to H_{0,0}) = 1 . \tag{4.27}$$

The probability distribution $\tilde{p}(\beta, n_{S_L})$ we want to sample is given by the weights of the configuration space $w(\beta, \omega)$ defined in Eq. 4.22. The ratio of probabilities can be written as

$$\frac{\tilde{p}(\beta, n_{S_L}+1)}{\tilde{p}(\beta, n_{S_L})} = \frac{w(\beta, \omega(n_{S_L}+1))}{w(\beta, \omega(n_{S_L}))} = \frac{\beta}{L - n_{S_L}} \cdot M_{ij} \ , \tag{4.28}$$

where M_{ij} is the eigenvalue of the inserted operator. According to the Metropolis Hastings algorithm, the acceptance probability for inserting a non-trivial operator is given by

$$a(H_{0,0} \to H_{i,j}) = \min\left(1, \ \frac{\tilde{p}(\beta, n_{S_L}+1)\, q(H_{i,j} \to H_{0,0})}{\tilde{p}(\beta, n_{S_L})\, q(H_{0,0} \to H_{i,j})}\right) \tag{4.29}$$

$$= \min\left(1, \ \frac{\beta}{L - n_{S_L}} \cdot M_{ij} \cdot \frac{\sum_i h_i + 2\sum_{i\neq j} |J_{ij}|}{M_{ij}}\right) \tag{4.30}$$

$$= \min\left(1, \ \frac{\beta\left(\sum_i h_i + 2\sum_{i\neq j} |J_{ij}|\right)}{L - n_{S_L}}\right) . \tag{4.31}$$

The acceptance probability for the opposite operation is analogously given by

$$a(H_{i,j} \to H_{0,0}) = \min\left(1, \ \frac{\tilde{p}(\beta, n_{S_L}-1)\, q(H_{0,0} \to H_{i,j})}{\tilde{p}(\beta, n_{S_L})\, q(H_{i,j} \to H_{0,0})}\right) \tag{4.32}$$

$$= \min\left(1, \ \frac{L - n_{S_L}+1}{\beta\left(\sum_i h_i + 2\sum_{i\neq j} |J_{ij}|\right)}\right) . \tag{4.33}$$

Note, that both of these probabilities do not depend on M_{ij}. Therefore, compared to the usual procedure in the Metropolis Hastings algorithm introduced in Sec. 4.1, steps 1 and 2 can be swapped. The algorithm can first decide whether an operator is to be exchanged using Eq. 4.31 or Eq. 4.33 by just drawing one random number and then which operator is to be used and whether the condition $H_{ij}|\alpha\rangle \neq 0$ is satisfied.

Walker method of aliases

An important part of the algorithm is to draw i, j according to their weight M_{ij}, i.e., to decide which operator is inserted because, in the case of the RTFIM, each operator can be inserted with a different probability $q(H_{0,0} \to H_{i,j})$. A method to draw random numbers from any discrete probability distribution in constant time is the Walker method of aliases [33].

To initialise the algorithm, the probabilities q_i are first divided into three groups. Probabilities greater than the mean probability $\bar{q}$, probabilities less than $\bar{q}$, and probabilities exactly equal to $\bar{q}$ [34]. Then, the probabilities are sorted into containers C_j and probabilities are redistributed until all containers are filled equally with at most two contributions from different samples [34] (see Fig. 4.3). It has to

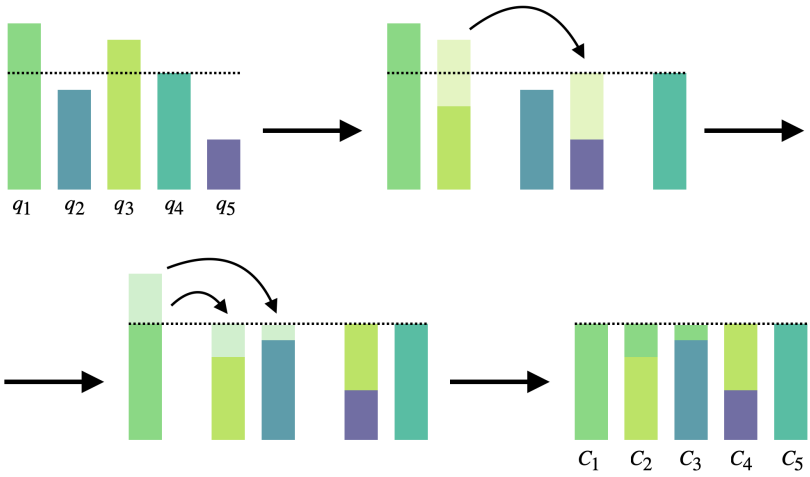

Figure 4.3: Initialisation of the Walker method: Probabilities q_i (coloured bars) are iteratively split up and assigned to containers C_i of equal size with contributions of one or two probabilities.

be saved which sample i a container C_j contains and their respective share. This initialisation needs at most as many steps as the number of q_i, but only has to be done once at the beginning of the simulation. To generate a sample from the distribution, only one *int* and one *double* random number need to be drawn from a uniform distribution. The first random number determines which container C_i is chosen, the second random number which of the two samples in the container is selected.

4.3.2 Off-diagonal update

In contrast to the diagonal update, the off-diagonal update does not change the weight of the configuration. Instead, the state of the system is updated by replacing constant operators $H_{i,i}$ with field operators $H_{i,0}$ and vice versa. This means that, among the other propagated states, also the initial state $|\alpha\rangle$ might change, which might affect the value of observables like the magnetisation. In this section two different updates are described, the local off-diagonal update, which only exchanges operators within the imaginary time of one single spin, and the quantum cluster update, which flips connected clusters of spins extending in both real space and imaginary-time dimension of the configuration.

Local off-diagonal update

In the local off-diagonal update, field operators are pairwise converted within the imaginary-time dimension of one spin, either from a constant operator $H_{i,i}$ into a field operator $H_{i,0}$ or the other way around. For this purpose, isolated local clusters, that are delimited by two field operators and have no Ising operator in between, are identified when going through the sequence and all spins in the local cluster are

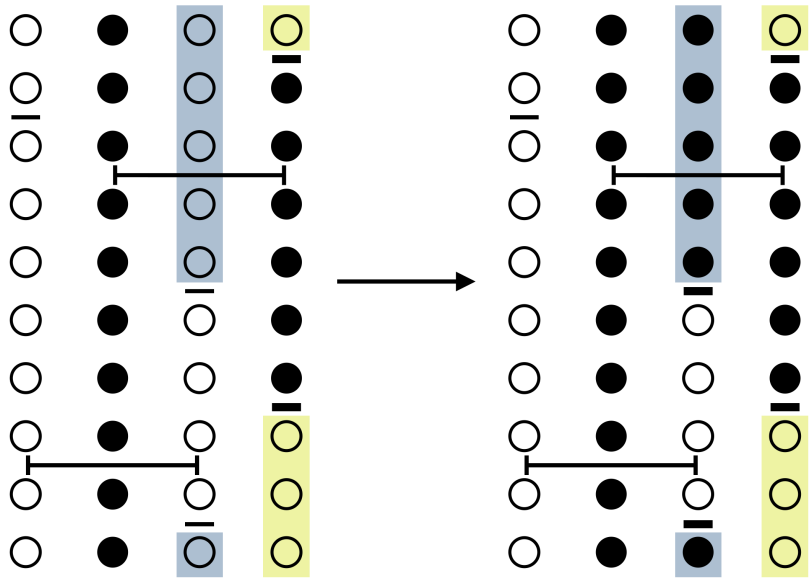

Figure 4.4: Construction of local isolated spin clusters represented by different colours. All spins of a local cluster are flipped with probability $p = 1/2$ during the local off-diagonal update.

flipped with probability $p = 1/2$ (see Fig. 4.4). This does not change the weight of the configuration, but the propagated states $|\alpha^{(k)}\rangle$. In particular, the initial state can also change if the cluster crosses the periodic boundary of imaginary time (see Fig. 4.4). Since this update only works locally, this update alone is not able to efficiently sample the configuration space close to the critical point. For this reason, only the cluster update described below was used for the simulations carried out in this work.

Quantum cluster update

The quantum cluster update differs from the local update in that the clusters are not limited to a single spin, but can expand in the dimension of real space by Ising operators, which connect the imaginary-time lines of two spins (see Fig. 4.5). As with the local off-diagonal update, the clusters are delimited by field and constant operators. For the cluster update, a doubly-linked vertex list is created during the diagonal update. It contains the information which operators are connected with each other, i.e., which operators are before and after an operator in imaginary time direction for every site. In the cluster update, all operators are visited with the help of this list and the clusters are constructed from it. Then, all spins of a cluster are flipped with probability $p = 1/2$ by replacing the constant operators at the cluster boundaries with field operators and vice versa. Detailed descriptions and implementation details can be found in Refs. [26, 30–32].

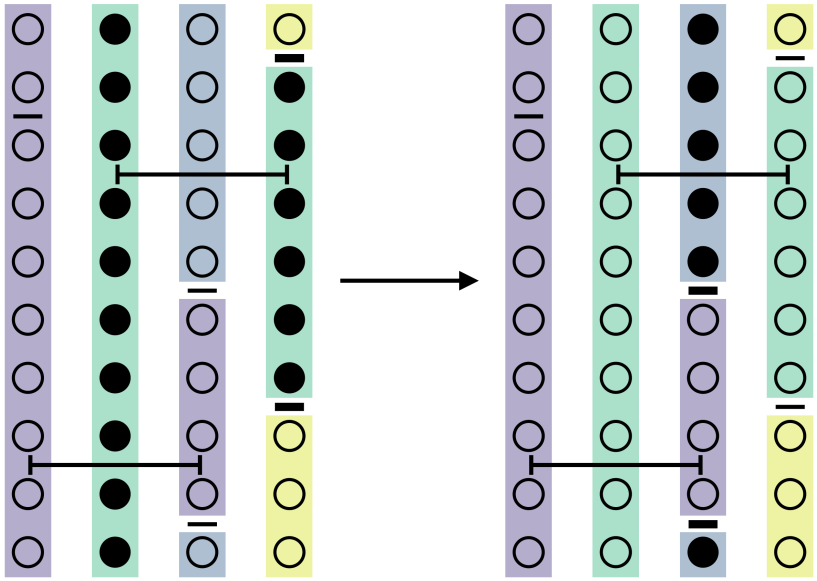

Figure 4.5: Construction of connected spin clusters represented by different colours. All spins of a cluster are then flipped with probability $p = 1/2$ during the quantum cluster update.

4.4 Calculation of observables

During each full update, observables are measured and in the end averaged over all Monte Carlo sweeps. Since some observables not only measure the initial state $|\alpha\rangle$ but also imaginary-time correlations and thus need access to all $|\alpha^{(k)}\rangle$, observables are measured during the diagonal update, since the whole sequence has to be traversed anyway.

First, an expression for the average energy, i.e., the ground-state energy, can be derived. The definition of the average energy can be expanded similar to the partition function [30]. Shifting $n \to n-1$ we recover the partition function with an additional factor $-n/\beta$:

$$E = \langle H \rangle = \frac{1}{Z} \mathrm{Tr}\left(He^{-\beta H}\right) \tag{4.34}$$

$$= \frac{1}{Z} \sum_{n=0}^{\infty} \frac{(-\beta)^n}{n!} \sum_{\{|\alpha\rangle\}} \langle\alpha| H^{n+1} |\alpha\rangle \tag{4.35}$$

$$= \frac{1}{Z} \sum_{n=1}^{\infty} \frac{(-\beta)^n}{n!} \cdot \frac{n}{-\beta} \sum_{\{|\alpha\rangle\}} \langle\alpha| H^{n} |\alpha\rangle \tag{4.36}$$

$$= \frac{1}{Z} \sum_{n=0}^{\infty} -\frac{n}{\beta} \cdot \frac{(-\beta)^n}{n!} \sum_{\{|\alpha\rangle\}} \langle\alpha| H^{n} |\alpha\rangle \ . \tag{4.37}$$

If we now apply the fixed-length scheme as described above, the ground-state energy in the SSE representation is given by the averaged number of non-trivial operators in the sequence divided by the inverse temperature

$$E = -\frac{\langle n_{S_L} \rangle_{w(\beta,\omega)}}{\beta} \ , \tag{4.38}$$

where $\langle ... \rangle_{w(\beta,\omega)}$ denotes the average over configurations sampled according to the weights $w(\beta, \omega)$ (see Eq. 4.22).

In general, any observables can be written as

$$\langle \mathcal{O} \rangle = \frac{1}{Z} \mathrm{Tr} \left(\mathcal{O} e^{-\beta H} \right) = \frac{1}{Z} \sum_{\{|\alpha\rangle\}} \sum_{n=0}^{\infty} \sum_{S_n} \frac{\beta^n}{n!} \langle \alpha | \, \mathcal{O} \prod_{l=1}^{n} H_{i(l),j(l)} \, |\alpha\rangle \tag{4.39}$$

in the SSE formalism. If the observable is diagonal in the chosen basis, one can further simplify the expression to

$$\langle \mathcal{O} \rangle = \langle \mathcal{O} \rangle_{w(\beta,\omega)} = \frac{1}{Z} \sum_{\omega \in \Omega} \mathcal{O}(\alpha) w(\beta, \omega) \ . \tag{4.40}$$

The statistics can be improved by using the fact that every rotated sequence is also a valid configuration [35]. The improved estimator of the observable $\mathcal{O}'$ does not only measure the state $|\alpha\rangle$, but also every propagated state $|\alpha^{(k)}\rangle$ for $k \in \{1, L-1\}$ in between:

$$\langle \mathcal{O}' \rangle_{w(\beta,\omega)} = \frac{1}{Z} \sum_{\omega \in \Omega} w(\beta, \omega) \frac{1}{L} \sum_{k=0}^{L-1} \mathcal{O}(\alpha^{(k)}) \ . \tag{4.41}$$

In the ferromagnetic RTFIM, the order parameter is given by the squared magnetisation

$$m^2 = \frac{1}{N^2} \Big(\sum_{i=1}^{N} \sigma_i^z \Big)^2 \ , \tag{4.42}$$

where N is the number of particles in the system. The expectation value of the squared magnetisation in the SSE representation

$$\langle m^2 \rangle_{w(\beta,\omega)} = \frac{1}{Z} \sum_{\omega \in \Omega} w(\beta, \omega) \frac{1}{L} \sum_{k=0}^{L-1} \langle \alpha^{(k)} | \, \frac{1}{N^2} \Big(\sum_{i=1}^{N} \sigma_i^z \Big)^2 \, |\alpha^{(k)}\rangle \tag{4.43}$$

is measured during the diagonal update by detecting field operators $H_{i,0}$ in the sequence, which change the propagated state. This means that the entire state of the system is not needed to be measured in each step k of the sequence, but the magnetisation can be constructed from the position of the field operators after the update.

The order parameter susceptibility is defined as the response function to an external magnetic field

$$\chi = N \int_0^\beta \langle m(\tau) m(0) \rangle d\tau \tag{4.44}$$

integrated over imaginary time. This integral can be expanded and expressed in terms of the SSE representation [30, 31] to

$$\chi = N \left\langle \frac{\beta}{n_{S_L}(n_{S_L}+1)} \left[\sum_{k=0}^{n_{S_L}-1} m_k^2 + \left(\sum_{k=0}^{n_{S_L}-1} m_k \right)^2 \right] \right\rangle_{w(\beta,\omega)} \tag{4.45}$$

with

$$m_k = \langle \alpha^{(k)} | m | \alpha^{(k)} \rangle \ . \tag{4.46}$$

The imaginary-time integrated correlation function

$$G_{ij} = \int_0^\beta \langle \sigma_i^z(\tau) \sigma_j^z(0) \rangle d\tau \tag{4.47}$$

$$= \left\langle \frac{\beta}{n_{S_L}(n_{S_L}+1)} \left[\sum_{k=0}^{n_{S_L}-1} \sigma_{i,k}^z \sigma_{j,k}^z + \left(\sum_{k=0}^{n_{S_L}-1} \sigma_{i,k}^z \right) \left(\sum_{k=0}^{n_{S_L}-1} \sigma_{j,k}^z \right) \right] \right\rangle_{w(\beta,\omega)} \tag{4.48}$$

with

$$\sigma_{i,k}^z = \langle \alpha^{(k)} | \sigma_i^z | \alpha^{(k)} \rangle \tag{4.49}$$

has a very similar form to the susceptibility. Both susceptibility and correlation functions are calculated during the diagonal update analogous to the magnetisation. In the case of the correlation function we have to restrict ourselves to the correlation function between one site $i = 1$ and all other sites j since calculating all correlations would slow down the simulation [31]. For the special case $i = j$, the imaginary-time integrated correlation function is equivalent to the local susceptibility

$$\chi_{\text{local}} = \int_0^\beta \langle \sigma_i^z(\tau) \sigma_i^z(0) \rangle d\tau \tag{4.50}$$

$$= \left\langle \frac{\beta}{n_{S_L}(n_{S_L}+1)} \left[n_{S_L} + \left(\sum_{k=0}^{n_{S_L}-1} \sigma_{i,k}^z \right)^2 \right] \right\rangle_{w(\beta,\omega)} \ . \tag{4.51}$$

This quantity is especially interesting since the distribution of the local susceptibility is connected to the distribution of typical energies and therefore gives us access to dynamical scaling (see Sec. 6.3).

4.5 Convergence to zero temperature

The aim of this work is to investigate continuous quantum phase transitions. However, quantum phase transitions are only defined at temperature $T = 0$ (see Sec. 2.1). In addition, continuous phase transitions only occur in the thermodynamic limit [14]. At first glance, this does not seem to fit well with the method described so far, which is only defined for finite systems and finite temperatures.

The key to solving this problem is to have a closer look at the behaviour of finite systems. In finite systems, in contrast to infinite systems, the energy gap Δ at the point of the phase transition does not close completely (see Sec. 5), but remains finite

$$\Delta(h = h_c, L) \sim L^{-z} \; . \tag{4.52}$$

In order to simulate the ground state, we only have to cool the system down so much that the remaining thermal fluctuations are very small compared to the energy gap to the first excited state.

Before the system at temperature T is simulated and observables can be measured, the system must first thermalise to the desired temperature $T = 1/\beta$. With decreasing temperature, the probability of inserting non-trivial operators in the sequence increases (see Eq. 4.31 and 4.33) and therefore also the fixed length L has to be increased in order to capture all relevant contributions of the configuration space.

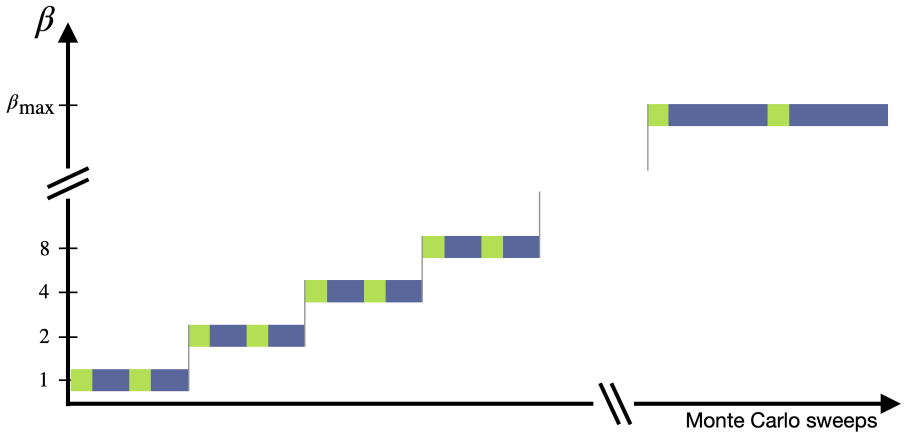

Figure 4.6: Visualisation of the beta-doubling method. In each step, beta is doubled and the system is twice thermalised (green) and twice observables are measured (blue). During the last step with the desired $\beta = \beta_{\max}$, more measurements are performed to obtain increased accuracy.

For this purpose, during the thermalisation process after every Monte Carlo sweep, it is checked whether the length $L \sim \beta N$ of the sequence is sufficient. If the condition $L > c{\cdot}n_{S_L}$ with $c > 1$ (e.g. $c = 1.25$) is not fulfilled, trivial operators are added to the

sequence until it is fulfilled again. This is carried out until the length of the sequence no longer changes. However, for very small temperatures it can take a long time for the system to thermalise. In addition, we do not know at the beginning what temperature is necessary to simulate the ground state of the system. Introducing the beta-doubling method, A. Sandvik [36] has given a way to tackle both of these problems. Here, we use an adapted version of this method.

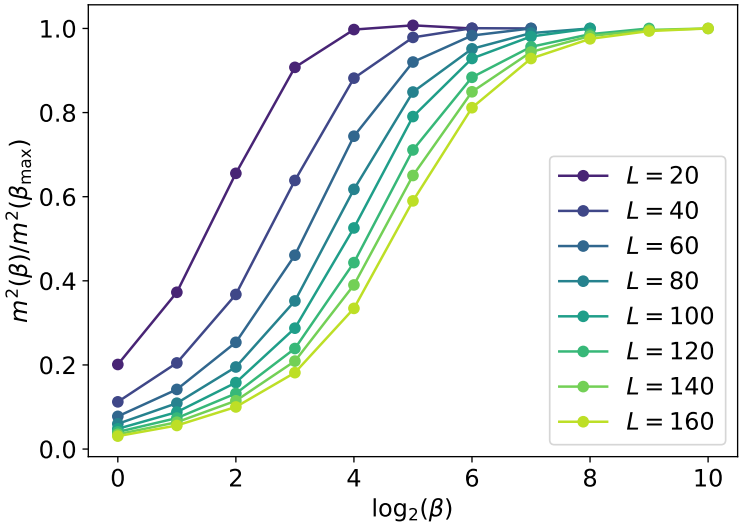

Figure 4.7: Averaged magnetisation curves of the RTFIC with different system size L for different inverse temperatures β.

Instead of starting the simulation at the desired temperature, the simulation begins in the first step at $\beta = 1$ and the β is doubled in each step. In every step the system is first thermalised before observables are measured. After that, the system is thermalised again and observables are measured a second time in this step to compare with the first measurement. If the two measurements do not coincide within statistical errors, the system was at least in the first step not equilibrated yet. Since $L \sim \beta$, the sequence of the system at half the temperature is expected to have a sequence twice as long. To shorten the thermalisation time in the next step, the doubled sequence

$$S_{2L}^{(2\beta)} = [S_L^{(\beta)}, S_L^{(\beta)}] \tag{4.53}$$

consisting of two copies of the previous sequence is used as initial sequence for the next beta step. Then the steps are repeated until the desired temperature is reached (see Fig. 4.6). At the lowest temperature, more Monte Carlo sweeps are taken in the measurements to get more accurate mean values, since these are the only measurements we use for further evaluation. Nevertheless, we need the intermediate measurements to check if we are converged to the ground state. In order to check this, the squared magnetisation was measured in each step and divided by the magnetisation from the last step with minimal temperature. If the system has been cooled down enough, this ratio converges to 1 as a function of β (see Fig. 4.7).

5 Finite-size scaling

In this thesis we want to investigate the critical behaviour of continuous quantum phase transitions. However, a sharp continuous phase transition with singularities only takes place in infinitely extended systems. Especially with disorder, it is very difficult to study a system in the thermodynamic limit. With the Quantum Monte Carlo method described in Sec. 4, we can only simulate finite systems. So how can we draw conclusions about an infinite system from the observables we measure in finite systems? The framework to solve this problem is called finite-size scaling. In the following, general finite-size scaling will be discussed, in particular how critical exponents can be extracted from different observables. Then, in Sec. 5.1, the special features of finite-size scaling in disordered quantum systems will be discussed, whereby we structurally follow the explanations in the appendix of Ref. [17]. Finally, the concrete method is presented with which we try to extract the critical point and correlation length exponents from our data.

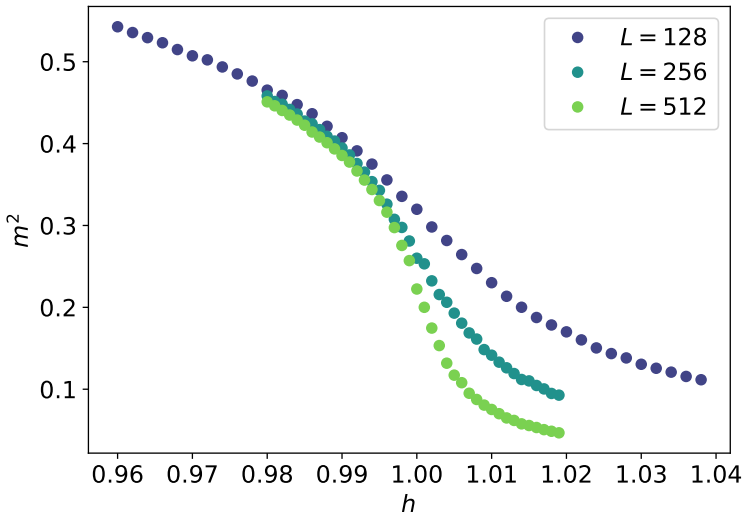

Figure 5.1: Magnetisation curves of the clean transverse-field Ising chain for different system sizes calculated with SSE quantum Monte Carlo. The sharp phase transition is rounded and shifted due to finite-size effects. Since the magnetisation does not diverge at the critical point, the shifting of the critical point is hardy visible with the eye.

Finite systems differ from infinite systems at the phase transition in that the critical point is shifted and the transition is no longer sharp but rounded [37] (see Fig. 5.1). According to the scaling hypothesis [38], thermodynamic quantities in the vicinity

of a phase transition behave like generalised homogeneous functions. The crucial point is that the scaling behaviour of observables with system size is related to the scaling of singular observables at the critical point of the infinite system. In other words, the critical exponents can be inferred from the behaviour of observables with the system size. In the quantum case, an observable $\mathcal{O}$ is expected to scale as

$$\mathcal{O}(r, L) = L^{-\omega/\nu} f_{\mathcal{O}}(rL^{1/\nu}) \ , \tag{5.1}$$

where ω is the critical exponent of the observable with respect to the order parameter and $f_{\mathcal{O}}$ a scaling function [39]. In particular, the scaling function for the order parameter in ferromagnetic Ising models, the squared magnetisation, is given by

$$m^2(r, L) = L^{-2\beta/\nu} f_{m^2}(rL^{1/\nu}) \ . \tag{5.2}$$

There are several techniques to extract the critical point and critical exponents from magnetisation curves. A frequently used method is a data collapse, where Eq. 5.2 is fitted to the magnetisation curves $m^2(r, L)$ of systems with different system sizes. From the best fit parameters, the critical point and exponents can be determined. After rescaling with the fit parameters found, the magnetisation curves should collapse to one curve, i.e., f_{m^2}. For the models investigated in this work, the application of a data collapse was not successful, probably because corrections to finite-size scaling (see e.g. Ref. [40]) are too large in this case. Instead, using the doubling method introduced in Sec. 5.2, the scaling of the distribution of pseudo-critical points, a quantity that is unique in disordered systems, is investigated. Moreover, we study the scaling behaviour of the magnetisation directly at the critical point.

5.1 Finite-size scaling in disordered quantum systems

The difference in finite systems with disorder is that observables must be averaged over many disorder realisations, i.e., not the scaling of a single value or curve but the scaling of distribution of values and curves must be considered. Often, the scaling of the distribution of the pseudo-critical points is investigated [41–44]. The finite-size critical point of a certain disorder realisation can be determined, e.g., by the maximum of a divergent variable such as the susceptibility or by the doubling method described in Sec. 5.2. Doing this for many disorder realisation, distributions of pseudo-critical points are obtained. The shift of the mean and the width of the distribution of pseudo-critical points then scale with exponents $\nu_{s/w}$ with the system size. But not every system with disorder behaves the same. A criterion for the stability of the critical point, the Harris criterion, was already discussed in Sec. 3.1. According to Refs. [17, 42], we can further subdivide the scaling behaviour into three groups.

Irrelevant disorder

As the name suggests, disorder is irrelevant for scaling in these systems. Systems falling into this group have a clean critical exponent ν_c that satisfies the Harris criterion. The scaling is analogous to the clean system without disorder described in the introduction to this chapter. For the scaling of the distribution of pseudo-critical points this means that the shift of the mean scales as $\sim L^{-1/\nu_s}$ with the clean exponent $\nu_s = \nu_c$, the width of the distribution according to the central limit theorem $\sim L^{-d/2}$ [42].

Conventional random scaling

If the Harris criterion is not met ($\nu_c < 2/d$), disorder is relevant. In the conventional case, which occurs in many systems such as diluted magnets or spin glasses [42], the universality class is changed. Using some assumptions, it can be shown that the exponent of the disordered system ν again satisfies the Harris criterion [16]. However, this statement is based on finite-size arguments and a finite-size correlation length ξ_{FS}. In general, it is not clear whether this definition agrees with that of the intrinsic correlation length ξ in the infinite system [16, 45]. The conventional case is characterised by the fact that densities still look homogeneous on large scales [17]. In renormalisation group language one says that the system has constant, non-vanishing strength of disorder under renormalisation. The typical energies scale similar to the clean system with $\Delta \sim L^{-z}$. Regarding the distribution of the pseudo-critical points, both, the shift of the mean and the width of the distribution, scale with the disorder exponent $\nu = \nu_s = \nu_w$.

Infinite random scaling

In addition to conventional scaling, there is the extreme case that the strength of the disorder becomes infinitely large under renormalisation. One speaks of the infinite disorder fixed point, where the disorder dominates over all quantum, thermal and statistical fluctuations [42, 46]. Examples of such systems include the RTFIM in one and two dimensions examined in this work. Here, the system does not look homogeneous even on large scales [17]. The reason for the strong disorder are the rare regions discussed in Sec. 3.2 having a large contribution to observables. As a result, a distinction must be made between average quantities dominated by rare regions and typical quantities. For the RTFIC, D. S. Fisher was able to show exactly using renormalisation group techniques that the average correlation length diverges with an exponent $\nu_{\text{av}} = 2$, whereas the typical correlation length diverges with an exponent $\nu_{\text{typ}} = 1$ at the phase transition [11]. Also the shift of the mean and the width of the distribution of pseudo-critical points does not have to scale with the same exponent, e.g., in the case of the RTFIC it scales with $\nu_s = 1$ and $\nu_w = 2$ (see [42] and Sec. 6.1.1).

The dynamical scaling behaves very peculiar. In contrast to conventional scaling, there is an exponential relationship between the typical energy scales and length scales

$$|\log \Delta| \sim \xi^{\psi} \qquad \rightarrow \qquad \Delta \sim \exp\left(cL^{\psi}\right) . \tag{5.3}$$

This is called activated scaling [11]. In particular, the activated scaling is a problem for our numerical simulation. As described in Sec. 4.5, we have to cool down our systems until the thermal energy is too small to generate excitations. Since the energy gap closes exponentially instead of polynomial with the system size, we have to cool down the system much more for larger system sizes, which has a negative effect on the performance of the simulation.

5.2 Scaling of pseudo-critical points: Doubling method

To study the scaling of the distribution of pseudo-critical points $P_{h_c}(L)$, it is important to precisely locate the pseudo-critical point of the finite systems. Only then, the mean and the width of the distribution can be determined for each system size with high accuracy. The exponents $\nu_{s/w}$ can be obtained by fitting

$$\langle h_c(L)\rangle_{P_{h_c}(L)} = h_c + A \cdot L^{-1/\nu_s} \qquad \sigma(P_{h_c}(L)) = B \cdot L^{-1/\nu_w} \tag{5.4}$$

to the data, where A and B are non-universal amplitudes and h_c is the critical point of the infinite system. Usually, physical quantities that diverge at the critical point, like the susceptibility, are used to define a sample-dependent critical point. However, the following sample-replication method turned out to deliver more precise estimates for a sample-dependent critical point. According to the doubling method [41], we calculate the magnetisation $m^2(h, L)$ of a certain system and also the magnetisation $m^2(h, 2L)$ of the doubled system, where we glue two copies of the first system together (see Fig. 5.2). Then the ratio of these magnetisations

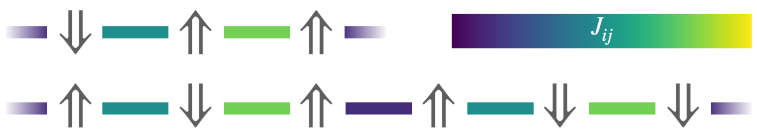

Figure 5.2: Visualisation of the simple system and doubled system of the RTFIC with bond disorder. The strength of the bonds J_{ij} is indicated by their colour. The doubled system consists of two times the simple system glued together at the boundaries.

$$r(h, L) = \frac{m^2(h, L)}{m^2(h, 2L)} \tag{5.5}$$

is investigated. In the case $h = 0$, the magnetisation of both the simple and the doubled system converges to one

$$\langle \Uparrow\Uparrow ... \Uparrow |m^2| \Uparrow\Uparrow ... \Uparrow\rangle = \langle \Uparrow\Uparrow ... \Uparrow |\frac{1}{L^2}\Big(\sum_i \sigma_i^z\Big)^2| \Uparrow\Uparrow ... \Uparrow\rangle \tag{5.6}$$

$$= \frac{1}{L^2}\sum_{i,j}\langle \Uparrow\Uparrow ... \Uparrow |\sigma_i^z\sigma_j^z| \Uparrow\Uparrow ... \Uparrow\rangle \tag{5.7}$$

$$= \frac{1}{L^2}\sum_{i,j} 1 = 1 \ . \tag{5.8}$$

In the case $h \to \infty$, the behaviour of the magnetisations can be shown analogous by rotating the coordinate system in the xz-plane ($\sigma^x \to -\sigma^z$ and $\sigma^z \to \sigma^x$) such that

$$\langle \Uparrow\Uparrow ... \Uparrow |m^2| \Uparrow\Uparrow ... \Uparrow\rangle = \langle \Uparrow\Uparrow ... \Uparrow |\frac{1}{L^2}\Big(\sum_i \sigma_i^x\Big)^2| \Uparrow\Uparrow ... \Uparrow\rangle \tag{5.9}$$

$$= \frac{1}{L^2}\langle \Uparrow\Uparrow ... \Uparrow |\Big(\sum_i (\sigma_i^x)^2 + \sum_{i\neq j}\sigma_i^x\sigma_j^x\Big)| \Uparrow\Uparrow ... \Uparrow\rangle \tag{5.10}$$

$$= \frac{1}{L^2}\Big(\sum_i 1 + \sum_{i\neq j} 0\Big) = \frac{1}{L} \ . \tag{5.11}$$

Therefore, the behaviour of the ratio $r(\alpha, L)$ is given by

$$\lim_{h\to\infty} r(h, L) \to \frac{1/2L}{1/L} = 1/2 \tag{5.12}$$

far in the disordered phase. We can now define the pseudo-critical point of a disorder realisation i as the values $h_c(i)$, where the ratio $r(h, L)$ drops from 1 to $1/2$. Doing this for many disorder realisations, we can calculate the mean and the width of the distribution of pseudo-critical points for different system sizes L. In Fig. 5.3, the typical behaviour of the ratio $r(h, L)$ is depicted for a few disorder realisations of the RTFIC with $L = 120$ spins. In the inset of Fig. 5.3 , a typical distribution of pseudo-critical points is depicted.

Since the decay is not sharp in small systems, it is not always easy to precisely determine the pseudo-critical point $h_c(i)$ of a disorder realisation i. After trying different methods, fitting a function

$$f(h) = \frac{1}{2}\left(\frac{1}{1 + \exp\left(a \cdot (h - h_c(i))\right)} + 1\right) \tag{5.13}$$

similar to a sigmoid function turned out to be the best. Other methods like interpolating between the data points to determine $r(h = h_c(i), L) = 0.75$ were also used. In general, the method used to determine the pseudo-critical point seems to affect the value h_c of the infinite system more than the exponents $\nu_{s/w}$.

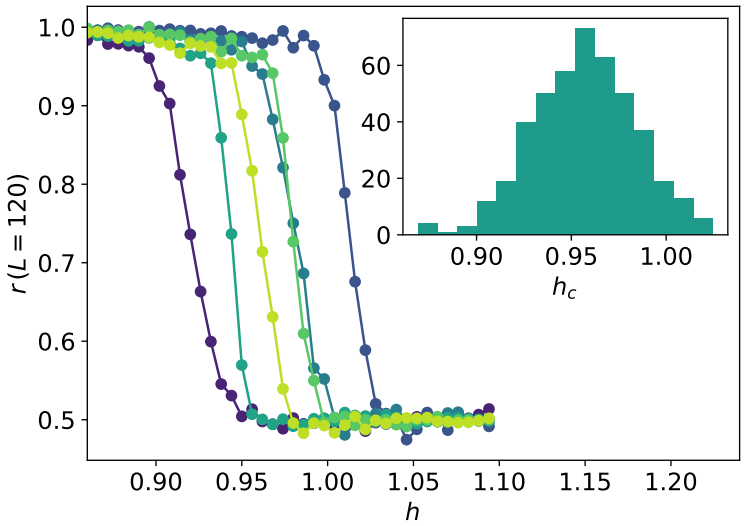

Figure 5.3: The ratio of magnetisations r for a few disorder realisations of the RTFIC with 120 spins and the corresponding doubled system calculated with the SSE quantum Monte Carlo method is shown. The pseudo-critical point is defined at the point where the ratio drops from 1 to 0.5. The distribution of pseudo-critical points (generated from more disorder realisations) is shown in the inset.

6 Results

In this chapter, the results for the critical behaviour of the RTFIM at $T = 0$ are presented. In Sec. 6.1, the scaling of the distribution of pseudo-critical points is examined using the doubling method described in Sec. 5.2. Critical points h_c and critical exponents $\nu_{s/w}$ are presented in one and two dimensions for different types of disorder. In Sec. 6.2 the averaged magnetisation at the critical point is considered to extract the order parameter critical exponent β. Finally, the dynamical scaling is examined using the behaviour of the local susceptibility in the Griffiths phase in Sec. 6.3.

Verification of the quantum Monte Carlo code

The code should first be verified using an exact method, since not only major errors can occur in the implementation, which lead to obviously wrong results, but also subtle errors can occur. Subtle errors in the code can lead to at first glance physical-looking results that are nevertheless wrong.

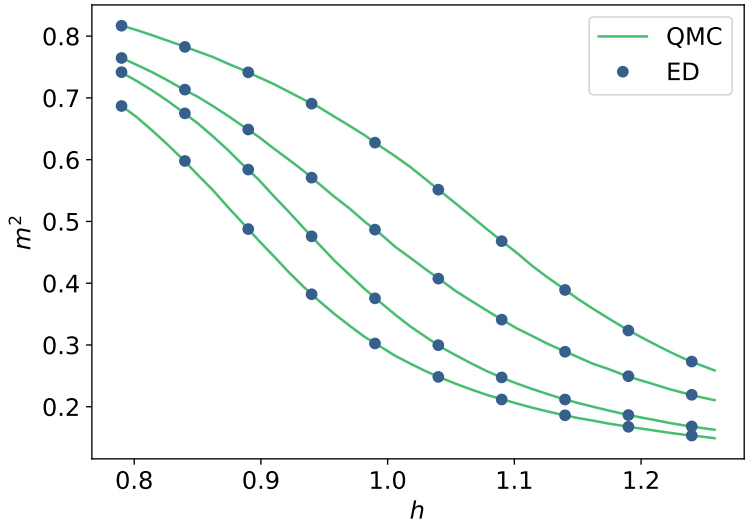

Figure 6.1: Magnetisation curves calculated for four disorder realisations of the RTFIC ($J_{ij} \in [0.5, 1.5]$) with 20 spins calculated with exact diagonalisation (ED) and SSE quantum Monte Carlo.

In order to rule out any errors in the implementation of the SSE quantum Monte Carlo method, the results of the code were compared to results from exact diagonalisation. In particular, this test was performed with disordered systems, since some

parts of the code differ from the implementation of clean systems. For the exact diagonalisation, the python package *QuSpin* [47] was used. With both methods, magnetisation curves were calculated for the same disorder configurations of the RTFIC (see Fig. 6.1), which agree very well.

6.1 Scaling of the distribution of pseudo-critical points

In this section, the scaling of the distribution of pseudo-critical points for one- and two-dimensional systems will be investigated. For this, we use the doubling method introduced in Sec. 5.2. The critical exponents and critical points are to be compared with already known results from literature [10, 11, 42, 44, 48]. In addition, it should be discussed which types of disorder are more suitable for the simulation with the quantum Monte Carlo method.

Verification of the method

The doubling method should also be compared with an exact method. For the chain we have the possibility to compare with the expression for the pseudo-critical point derived in Sec. 3.3.1 [10]. In two dimensions we do not have this possibility. However, we assume that once the method has been verified for one-dimensional systems it can also be applied to two-dimensional systems.

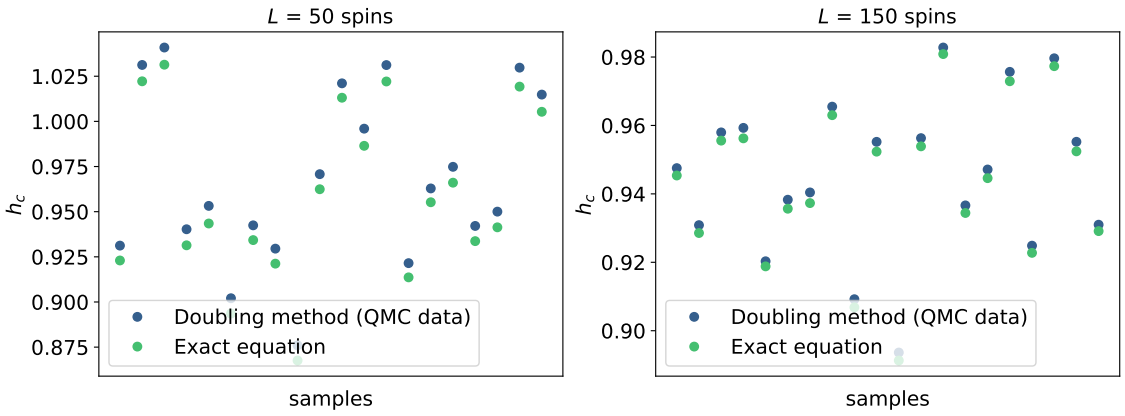

Figure 6.2: Position of the pseudo-critical point extracted via the doubling method using quantum Monte Carlo data compared to pseudo-critical point determined using Eq. 3.36. The deviation between the points is decreasing with increasing system size.

In Fig. 6.2 the pseudo-critical points of 20 disorder realisations of the RTFIC are plotted, once calculated with SSE and the doubling method and once using Eq. 3.36

from the bond strengths of the disorder realisations. One can see that the pseudo-critical points of the different methods are correlated and very close to each other. A systematic shift between the points can be seen, which becomes smaller as the system size increases. The reason for this could be the boundary term neglected in the exact calculation for the value of the pseudo-critical point. This is consistent with the assumption that the contribution from the boundary term is negligible for very large systems. However, it cannot be ruled out that determining the pseudo-critical point using Eq. 5.13 also leads to an error that disappears in the limit of large systems.

6.1.1 Results for the one-dimensional RTFIM

The one-dimensional model, i.e. the RTFIC, is the simplest realisation of the RTFIM and also the one best studied in literature [10, 11, 42, 49, 50]. Therefore it is a good starting point for our method, since we can easily compare our results. On the one hand, we can use Eq. 3.36 [10] to calculate distributions of critical exponents for very large systems with little computational effort and thus make good predictions for the critical point of the infinite system h_c. On the other hand, D. S. Fisher was able to use renormalisation group techniques to show that the average and typical correlation length of the chain diverges with $\nu_{\text{av}} = 2$ and $\nu_{typ} = 1$ and that the order parameter exponent is given by $\beta = \frac{1}{2}(3 - \sqrt{5})$ [11].

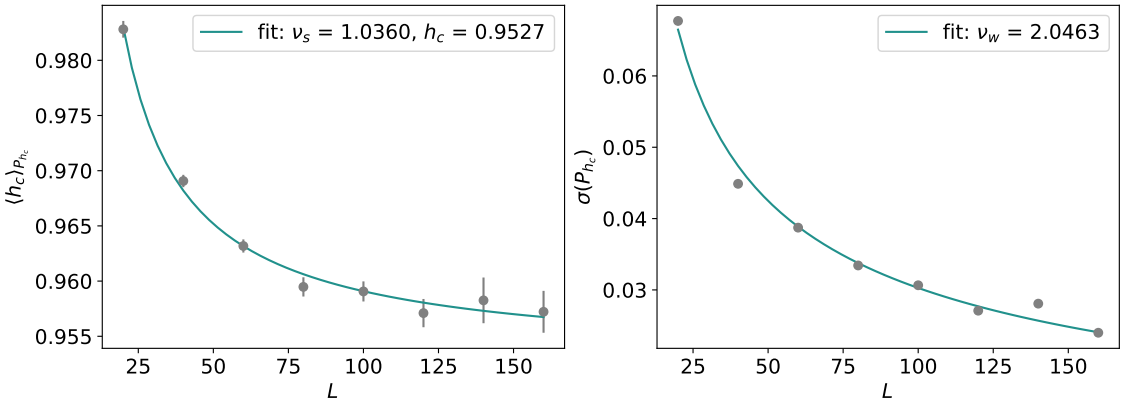

Figure 6.3: Scaling of mean and width of the distribution of pseudo-critical points using SSE data. The investigated system is the RTFIC with bond disorder $J_{ij} \in [0.5, 1.5]$.

Regarding the distribution of pseudo-critical points, F. Igloi et al. showed that the mean and width of the distribution scale with exponents $\nu_s = 1$ and $\nu_w = 2$ [42] and connected those to the exponents of average and typical correlations. However, it is unclear whether these exponents can be related in general.

In this work, the chain was simulated for three different types of disorder:

- Bond strengths J_{ij} drawn from a unitary distribution [0.5,1.5] and no disorder in $h_i = h$ (see Fig. 6.3)
- Bond strengths J_{ij} drawn from a unitary distribution [0,1] and no disorder in $h_i = h$ (see Fig. 6.4)
- Bond strengths J_{ij} drawn from a unitary distribution [0,1] and field strengths h_i drawn from a distribution $[0, h]$ (see Fig. 6.5)

For the first two types of disorder, the bond strengths were kept constant during the simulation and the system was simulated for different values of h. In the case of disorder in the bond and field strengths, a configuration of $\{J_{ij}, h_i\}$ was drawn from [0,1] at the beginning of each simulation of a disorder realisation. To change the ratio $\langle J_{ij}\rangle/\langle h_i\rangle$, the h_i were rescaled with h. The three types of disorder were chosen such that they can be compared well with literature [42], but also to investigate how different types of disorder behave. The disorder seems to be more "extreme" if the bonds are chosen to be in $[0, 1]$ instead of $[0.5, 1.5]$, as this allows $J_{ij} \approx 0$ to occur, which could split up the system. Disorder in the field strengths further increases the strength of the disorder.

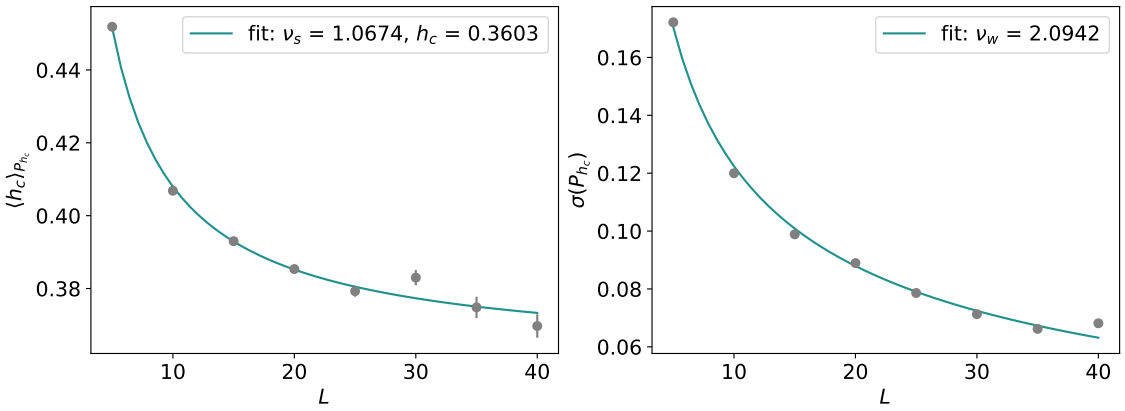

Figure 6.4: Scaling of mean and width of the distribution of pseudo-critical points using SSE data. The investigated system is the RTFIC with bond disorder $J_{ij} \in [0, 1]$.

In Fig. 6.3 and Fig. 6.4 one can see that the exponents $\nu_{s/w}$ agree well with the results of [42] despite some statistical inaccuracy. Moreover, the position of the critical points agrees quite well with the estimates one gets using Eq. 3.36

$$h_c(J_{ij} \in [0.5, 1.5]) \approx 0.956 \qquad h_c(J_{ij} \in [0, 1]) \approx 0.368\ . \tag{6.1}$$

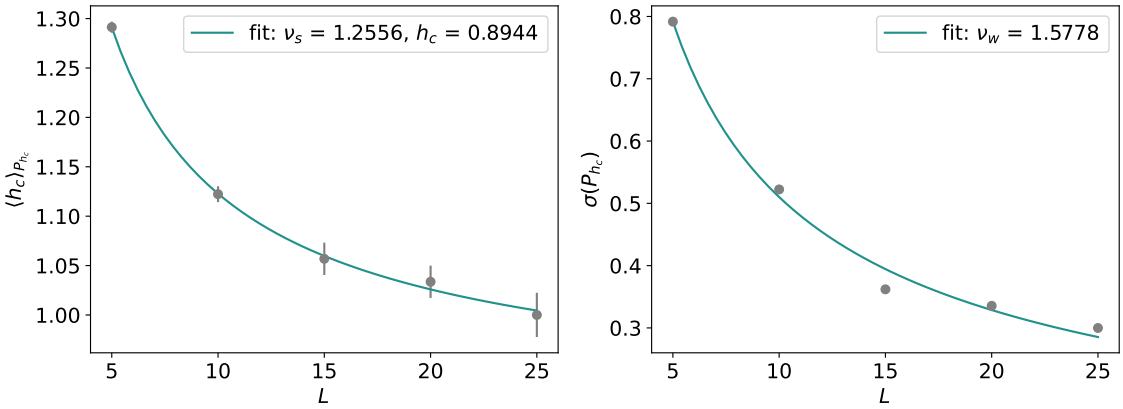

Figure 6.5: Scaling of mean and width of the distribution of pseudo-critical points using SSE data. The investigated system is the RTFIC with bond disorder $J_{ij} \in [0, 1]$ and field disorder $h_i \in [0, h]$.

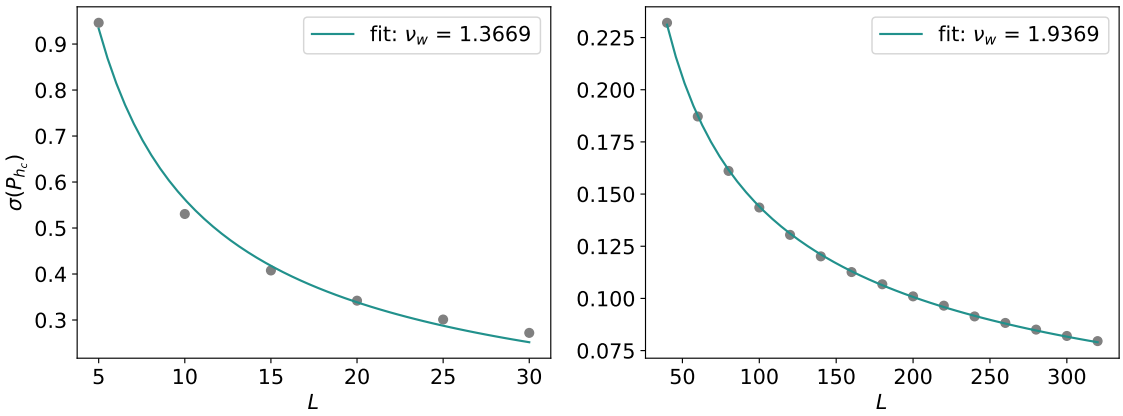

Figure 6.6: Scaling the width of the distribution of pseudo-critical points for the RTFIC with bond disorder $J_{ij} \in [0, 1]$ and field disorder $h_i \in [0, h]$. Here Eq. 3.35 was used to determine the distribution of pseudo-critical points.

In contrast, the exponents for the case of disorder in bonds and field strengths still deviate from the expected results, especially with regard to the width of the distribution (see Fig. 6.5). Reason for this is probably that we calculated too small system sizes in this simulation. The problem with "stronger" disorder seems to be that the activated scaling (see Eq. 5.3) becomes more important. This results in exponentially small energy gaps with increasing system sizes such that we have to go to very low temperatures even with comparably small systems. This makes it difficult to simulate large systems with enough disorder realisations and thus to obtain data points with good statistics in a reasonable amount of computing time.

To check this assumption, we used Eq. 3.35 and determined the distribution of pseudo-critical points for disorder in J and h. The scaling of the width of the distribution can be seen in Fig. 6.6 on the left for small system sizes comparable to those from the SSE simulation. Here the exponent deviates strongly from the expected exponent $\nu_w = 2$ as well. In contrast, the exponent is close to the expected value for larger systems in Fig. 6.6 on the right. However, it cannot be ruled out that the neglected boundary term also influences the comparison.

6.1.2 Results for the two-dimensional RTFIM

In two dimensions, the RTFIM on the square lattice was considered. Less is known here in contrast to the chain. There are no exact results for the comparison of critical points and exponents, but a work by I. A. Kovacs et al., who found exponents $\nu_s = \nu_w \approx 1.24$ for the distribution of pseudo-critical points using strong disorder renormalisation group techniques [44]. C. Monthus et al. found similar results $\nu \approx 1.3$ using the same technique [48].

In our simulation, two different types of disorder were simulated:

- Bond strengths J_{ij} drawn from a unitary distribution [0.5,1.5] and no disorder in $h_i = h$ (see Fig. 6.7)
- Bond strengths J_{ij} drawn from a unitary distribution [0,1] and field strengths h_i drawn from a distribution $[0, h]$ (see Fig. 6.8)

The latter type of disorder was also investigated in [44], so we can compare with their results. In Fig. 6.7 and Fig. 6.8 one can see that it is quite difficult to determine the shift exponent ν_s from our data because the statistical fluctuations are very large.

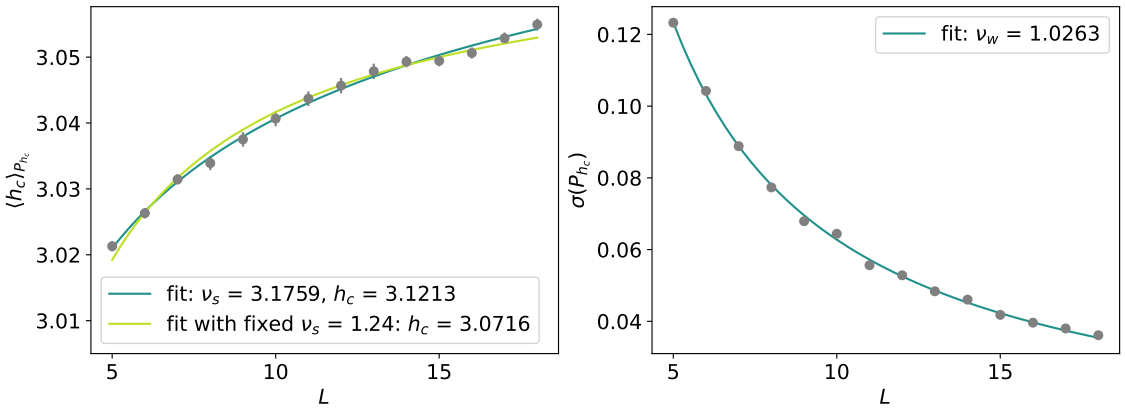

Figure 6.7: Scaling of mean and width of the distribution of pseudo-critical points using SSE data. The investigated system is the RTFIM on the square lattice with bond disorder $J_{ij} \in [0.5, 1.5]$.

On the other hand, a fit with fixed $\nu_s = 1.24$ is nevertheless consistent with the data points. For the width exponents, the data points look more converged, but we can not reproduce $\nu_w = 1.24$ with sufficient accuracy.

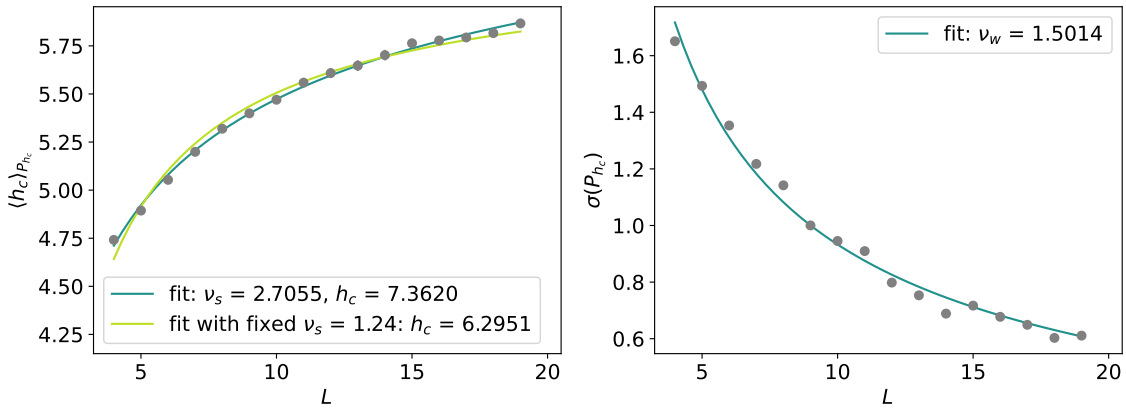

Figure 6.8: Scaling of mean and width of the distribution of pseudo-critical points using SSE data. The investigated system is the RTFIM on the square lattice with bond disorder $J_{ij} \in [0, 1]$ and field disorder $h_i \in [0, h]$.

In Ref. [44], a finite-size dependency of the exponents was considered. In the case where there is only disorder in the bond strengths, the exponents $\nu_{s/w}$ converge to 1.24 with increasing system size L from below. In the case where there is disorder in bond and field strengths, it converges from above [44]. This is in agreement with our results for the exponents ν_w in Fig. 6.7 and Fig. 6.8. We further analysed this L-dependency of the exponent due to the corrections to finite-size scaling. In Fig. 6.9, the data point of the smallest system size was removed in each step and the exponents were determined for the remaining system sizes in each step. One can see that both exponents become smaller and tend to converge towards 1.24 although the error bars are quite large, especially in the case of ν_s. This is where the advantage of stronger disorder becomes apparent. While the convergence to the correct exponents in Fig. 6.9 can be seen well, it could not be proven for the model with only disorder in the bond strengths within the available system sizes. This is also in agreement with Ref. [44], where they showed that the convergence for the model with only disorder in the bond strengths appeared at significantly larger system sizes.

Comparing the obtained value of the critical point of the infinite system h_c from Fig. 6.8 with the value $h_c \approx 5.37$ of Ref. [44], a big difference is noticeable that is too large to be due to statistical inaccuracies. Renormalisation group techniques, as applied to the RTFIM in Refs. [44, 48], archive very precise results for universal quantities like critical exponents, but do not necessarily predict the "true" sample dependent critical point [51], since microscopic details are lost in the renormalisation process [52]. The best estimate for the critical point from our data can be archived by a fit in which the known critical exponent $\nu_s = 1.24$ is fixed (see Fig. 6.8). We obtain

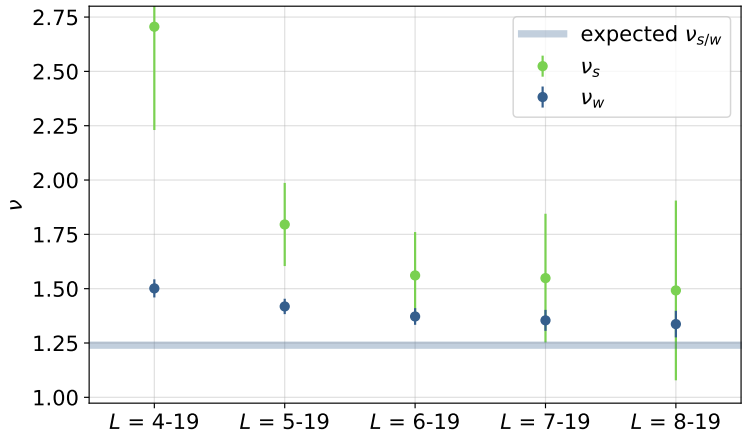

Figure 6.9: In each step the data point of the smallest system size is removed and fits for the remaining data points are performed. One can see, that the exponents $\nu_{s/w}$ are L dependent and tend to converge to the expected value $\nu_{s/w} \approx 1.24$ [44]. The investigated system is the RTFIM on the square lattice with bond disorder $J_{ij} \in [0, 1]$ and field disorder $h_i \in [0, h]$.

$h_c \approx 6.30$, which is probably closer to the "true" critical point since the quantum Monte Carlo method, unlike the strong disorder renormalisation group technique [53], also captures the microscopic details that are relevant for the position of the critical point.

6.2 Scaling of the magnetisation at the critical point

According to Eq. 5.2, the averaged, squared magnetisation at the critical point ($r = 0$) is expected to scale like

$$\langle m^2(r = 0, L)\rangle \sim L^{-2\beta/\nu_{\text{av}}} \ . \tag{6.2}$$

For the chain, we can determine the critical point h_c to high accuracy. For the square lattice, we use the critical points obtained from the doubling method. In both cases, the averaged magnetisation at the critical point $\langle m^2(h = h_c, L)\rangle$ was plotted logarithmically against the system size L, so that the exponent $2\beta/\nu_{\text{av}}$ can be read off via a linear fit. In addition, a second quantity is examined to extract only the average correlation length exponent ν_{av} by expanding the scaling function close to the critical point

$$1 - \frac{\langle m^2(r = \delta)\rangle}{\langle m^2(r = 0)\rangle} = 1 - \frac{L^{-2\beta/\nu_{\text{av}}} f(\delta L^{1/\nu_{\text{av}}})}{L^{-2\beta/\nu_{\text{av}}} f(0)} \tag{6.3}$$

$$= 1 - \frac{f(0) + \frac{\partial f}{\partial \delta}|_{\delta=0} \delta L^{1/\nu_{\text{av}}} + O(\delta^2)}{f(0)} \sim L^{-1/\nu_{\text{av}}} \ . \tag{6.4}$$

The behaviour of both quantities can be seen in Fig. 6.10 for the chain and in Fig. 6.12 for the square lattice.

In the case of the chain with disorder in bond and field strengths, the analytically known exponent $\beta = \frac{1}{2}(3 - \sqrt{5}) \approx 0.382$ [11] roughly agrees with our results. Deviations in both cases may be due to corrections to finite-size scaling and too few disorder realisations. We can actively try to take these corrections into account. To do this, the data points $\log \langle m^2(h_c) \rangle$ are multiplied with $\log(L)$ and a quadratic function was fitted to the data instead of a linear function. Therefore we have one more degree of freedom to take corrections into account. In Fig. 6.11, one can see that the exponents agree much better with the literature values $\beta \approx 0.382$ and $\nu_{\text{av}} = 2$ using the quadratic fit.

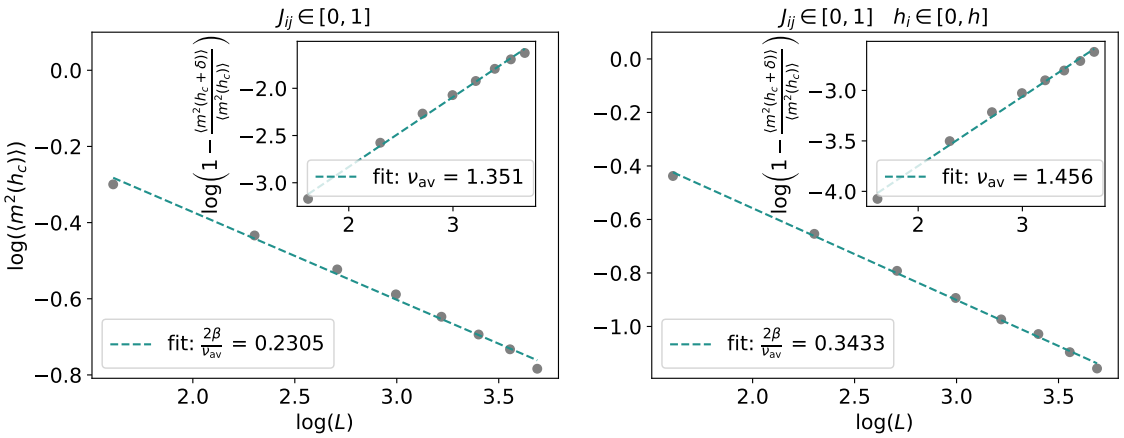

Figure 6.10: Scaling of the average magnetisation of the RTFIC at the critical point for two different types of disorder in order to extract the exponents β and ν_{av}.

For the square lattice, we can compare our results with Ref. [44], according to which $2\beta/\nu_{\text{av}} \approx 1.964$. Unfortunately, our results do not match this value. Also the correlation length exponent $\nu_{\text{av}} = 1.24$ [44] can not be reproduced with sufficient accuracy. This is probably due to several reasons. On the one hand, as with the doubling method, the system sizes are too small, so that corrections to finite-size scaling influence the exponents. In order to effectively include these in a fit, however, the data points still fluctuate too much. Also the method that was used for the linear chain to take corrections into account does not improve the results. Probably the correction do not have the same form in the two-dimensional system. On the other hand, in contrast to the chain, we cannot determine the critical point to high accuracy. Scaling away from the critical point will massively influence the exponents.

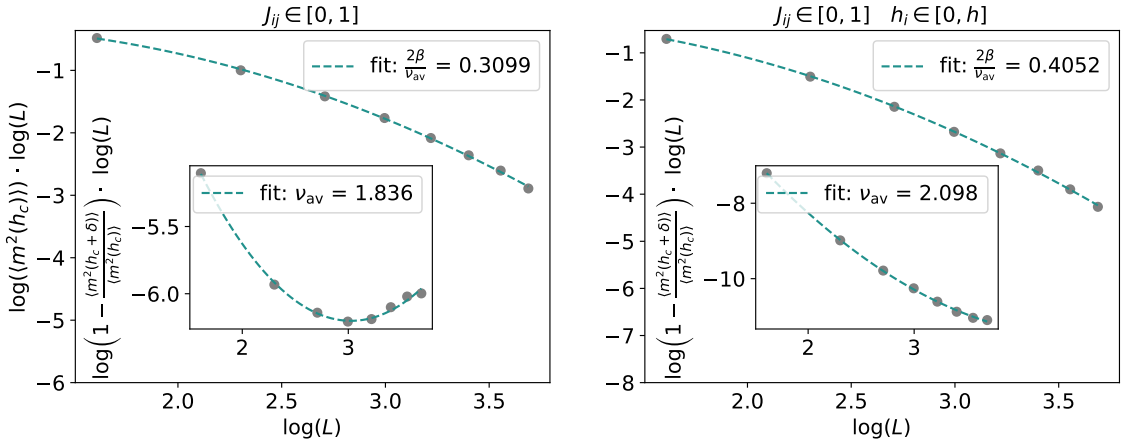

Figure 6.11: Scaling of the average magnetisation of the RTFIC at the critical point for two different types of disorder in order to extract the exponents β and ν_{av}. Here, the data points are multiplied with $\log L$ and a quadratic fit is performed instead to take corrections to finite-size scaling into account.

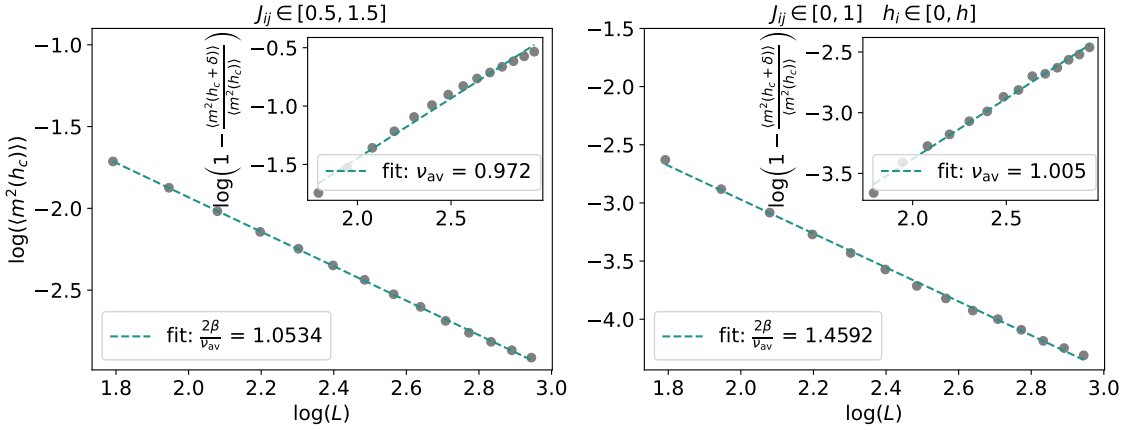

Figure 6.12: Scaling of the average magnetisation of the RTFIM on the square lattice at the critical point for two different types of disorder in order to extract the exponents β and ν_{av}.

6.3 Dynamical scaling in the Griffiths phase

In the following section, dynamical scaling in the paramagnetic Griffiths phase will be investigated. As described in Sec. 3.2, rare regions dominate the observables and properties in this phase. From the distribution of the linear size L_R of the rare regions (see Eq. 3.5) and the relation between energy gap Δ and L_R (see Eq. 3.7), the distribution of the energy gaps in the limit of small Δ can be determined

$$P(\Delta) \sim P(L_R(\Delta)) \cdot \frac{dL_R}{d\Delta} = e^{\frac{\alpha}{\sigma}\log\Delta} \cdot \frac{-\sigma}{\Delta} \sim \Delta^{\frac{\alpha}{\sigma}-1} = \Delta^{\frac{d}{z'}-1} , \tag{6.5}$$

where α/σ was identified with d/z'. Analogous to the critical exponent z introduced in Sec. 2.2, z' also relates typical energies and typical lengths, but this time for rare regions in the Griffiths phase. d is the dimension of the system. This quantity can

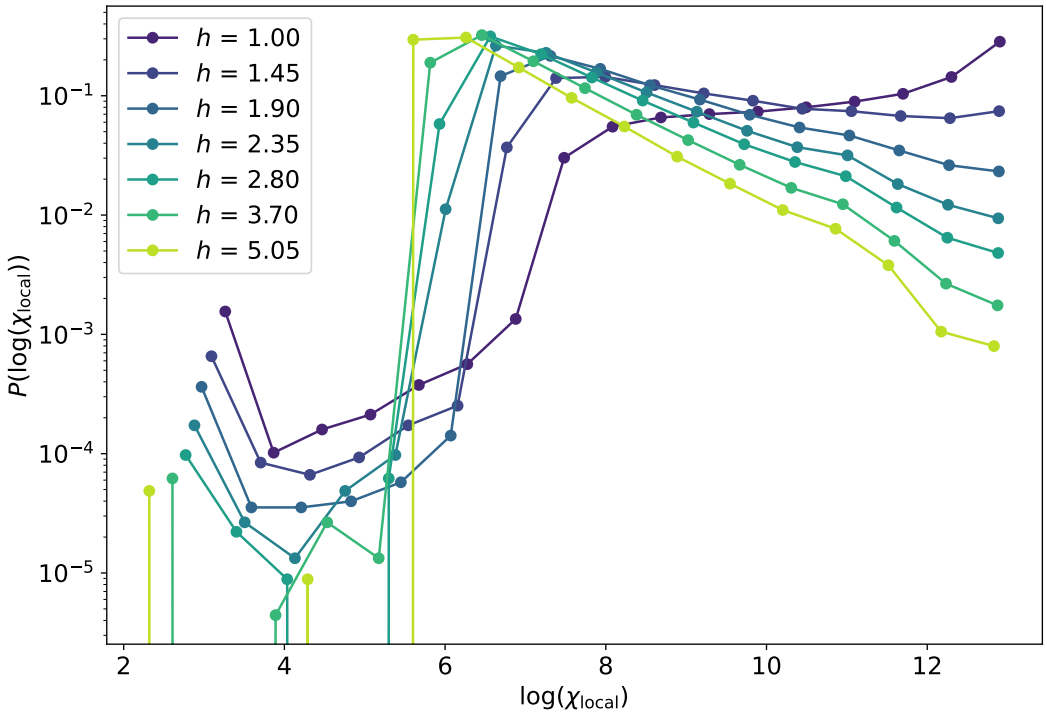

Figure 6.13: Distribution of the local susceptibility calculated using SSE data for different values of h. The investigated system is the RTFIC with bond disorder $J_{ij} \in [0, 1]$ and field disorder $h_i \in [0, 1]$.

be connected to the local susceptibility defined in Eq. 4.50

$$\chi_{\text{local}} = \int_0^\beta \langle \sigma_i^z(\tau)\sigma_i^z(0)\rangle \tag{6.6}$$

$$= \int_0^\beta \langle 0|e^{H\tau}\sigma_i^z e^{-H\tau}\sigma_i^z|0\rangle \ . \tag{6.7}$$

By inserting $\mathbb{1} = \sum_{n\neq 0} |n\rangle\langle n|$, where $|n\rangle$ denotes a many body state of the system, we end up with

$$\chi_{\text{local}} = \int_0^\beta \sum_{n\neq 0} \langle 0|e^{H\tau}\sigma_i^z e^{-H\tau}|n\rangle\langle n|\sigma_i^z|0\rangle \tag{6.8}$$

$$= \sum_{n\neq 0} \int_0^\beta e^{-\tau(E_n-E_0)}\langle 0|\sigma_i^z|n\rangle\langle n|\sigma_i^z|0\rangle \tag{6.9}$$

$$= \sum_{n\neq 0} \left[\frac{-1}{E_n-E_0} e^{-\tau(E_n-E_0)}\right]_0^\beta |\langle 0|\sigma_i^z|n\rangle|^2 \tag{6.10}$$

$$= \sum_{n\neq 0} \frac{|\langle 0|\sigma_i^z|n\rangle|^2}{E_n-E_0}\left(1-e^{-\beta(E_n-E_0)}\right) \ . \tag{6.11}$$

For sufficiently large β the local susceptibility we measure is therefore proportional to $1/\Delta$

$$\chi_{\text{local}} \sim \frac{1}{E_n-E_0} \sim \frac{1}{\Delta} \tag{6.12}$$

and the tail of the distribution of the local susceptibility scales as

$$P(\chi_{\text{local}}) = P(\Delta(\chi_{\text{local}}))\frac{d\Delta}{d\chi_{\text{local}}} \sim \chi_{\text{local}}^{-d/z'+1} \ . \tag{6.13}$$

During our simulation of the RTFIM in one and two dimensions we also calculated χ_{local} for each spin on the respective lattice. In order to extract the exponent d/z', the logarithm of the distribution of χ_{local} was plotted against the logarithm of χ_{local} (see Fig. 6.13). One can see that the logarithm of the distribution for large values of χ_{local} shows a linear behaviour. This range corresponds to very small energy scales or large relaxation times, i.e., the range dominated by rare regions, where Eq. 6.13 is valid. Especially in the case $h \approx h_c$ one can see, that the linear behaviour is disturbed. This is probably due to the fact that $\beta < \infty$. For observables close to the critical point, Δ is very small and thus the additional term in Eq. 6.11 may contribute. To determine d/z', linear curves are fitted to the tails of the distribution. Since

$$\log\left[P(\log\chi_{\text{local}})\right] \sim -\frac{d}{z'}\log\chi_{\text{local}} \ , \tag{6.14}$$

d/z' is determined from the slope. The behaviour of d/z' with the field strength h is plotted in Fig. 6.14 for a one- and a two-dimensional system with linear system size $L = 16$ each. For both the one-dimensional and the two-dimensional model, we see that the exponent z' diverges close to the point of the phase transition and approaches a constant value for large fields h. This is in good agreement with previous works that have demonstrated the same behaviour [49, 54]. The reason for this behaviour is that in the Griffiths phase conventional scaling $\delta \sim \xi^{-z}$ is

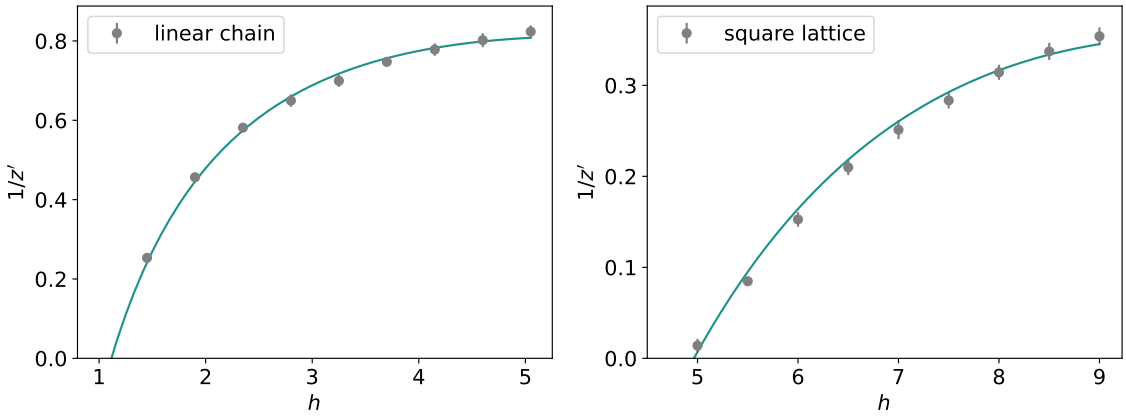

Figure 6.14: Exponent z' in the Griffiths phase extracted from the distribution of the local susceptibility for the RTFIM in one (left) and two (right) dimensions, both with linear system size $L = 16$. In both cases, the type of disorder is $J_{ij} \in [0, 1]$ and $h_i \in [0, h]$.

expected, while at the critical point activated scaling ($z = \infty$) is expected (see Sec. 5.1) [17]. It is noticeable that the point $h(1/z' = 0)$ deviates from the critical point h_c. If the simulations are carried out for different system sizes L, one can see that $h(1/z' = 0, L)$ is also influenced by finite-size effects. The finite-size pseudo-critical points, which can be determined by $h(1/z' = 0, L)$, do not generally agree with those determined by the doubling method.

7 Conclusion and Outlook

In this work, the critical behaviour at the phase transition of the random transverse-field Ising model was investigated in one and two dimensions. For this purpose, the ground state of the RTFIM was simulated using stochastic series expansion Monte Carlo [13]. Using the beta doubling method [36], observables at $T = 0$ could be extracted for finite systems.

To investigate the scaling behaviour, different techniques were applied. First, a sample replication technique [41] was used to determine the pseudo-critical point of individual disorder realisations. From the scaling behaviour of the distribution of pseudo-critical points, the exponents $\nu_{s/w}$ and the critical point h_c were extracted. In one dimension, the results agree very well with the analytical values for h_c [10] and the critical exponents of Ref. [42]. One can see that due to corrections to finite-size scaling, the convergence to the true exponents depends on how exactly the disorder is chosen in the model. In two dimensions it is more difficult to determine exponents and critical points with sufficient precession, since the simulation becomes more time-consuming for the same linear system sizes and thus fewer disorder realisations can be determined in the same time. We see that in the range of the system sizes we simulated, the exponents have not yet converged to their true values. However, we observe consistent behaviour of the L-dependent critical exponents and a convergence towards the exponents $\nu_{s/w} = 1.24$ determined by Ref. [44]. The critical point h_c deviates strongly from those determined by strong disorder renormalisation group techniques [44, 48]. This is probably not only due to statistical inaccuracies but also due to the fact that our estimates for the critical points are not biased in contrast to the renormalisation group method.

To determine the order parameter critical exponent β, the averaged magnetisation at the critical point was considered. In one dimension, the exponent we determine agrees well with the exact value $\beta = \frac{1}{2}(3 - \sqrt{5})$ [11]. Again, the result is strongly dependent on the type of disorder we consider and corrections to finite-size scaling have a great impact. In two dimensions, it was not possible to reproduce the results for β from Ref. [44]. The reason for this is probably that we have too many inaccuracies and corrections due to too small system sizes and too few disorder realisations, but also that we do not know the exact position of the critical point in the two-dimensional model.

Finally, the behaviour of the distribution of the local susceptibility in the disordered Griffiths phase was examined. This quantity is related to the distribution of typical energies and has an algebraic tail that decays with d/z'. The behaviour of the critical exponent z' with the field strength h was investigated and shows the expected behaviour in one and two dimensions [49, 54]. At the point of the phase transition, z' diverges according to activated scaling. For large h the dynamical exponent z' has a constant value.

It turned out, that the activated scaling of disordered quantum systems worsens the performance of the quantum Monte Carlo method, because we have to simulate at lower temperatures compared to the clean system. Although our results are still influenced by statistical uncertainties, we showed in this work that SSE quantum Monte Carlo is a suitable method to simulate the RTFIM and to obtain unbiased results for critical exponents and critical points.

For future projects, it would be interesting to investigate whether we can improve our methods to generate as many disorder realisations as possible and to determine pseudo-critical points with higher precision. One idea would be to use quasi-random sequences instead of pseudo-random numbers in order to converge faster towards mean values. If it is possible to further optimise the simulations for the square lattice, it would be interesting to investigate the interplay of disorder and frustration with systems such as the antiferromagnetic triangular or Kagome lattice.

8 Bibliography

[1] D. Thouless, "Electrons in disordered systems and the theory of localization", Physics Reports **13**, 93 (1974) (cit. on p. 1).

[2] T. Vojta, "Disorder in quantum many-body systems", Annual Review of Condensed Matter Physics **10**, 233 (2019) (cit. on p. 1).

[3] P. W. Anderson, "Absence of diffusion in certain random lattices", Phys. Rev. **109**, 1492 (1958) (cit. on p. 1).

[4] D. Basko, I. Aleiner, and B. Altshuler, "Metal–insulator transition in a weakly interacting many-electron system with localized single-particle states", Annals of Physics **321**, 1126 (2006) (cit. on p. 1).

[5] M. Hörmann, P. Wunderlich, and K. P. Schmidt, "Dynamic structure factor of disordered quantum spin ladders", Phys. Rev. Lett. **121**, 167201 (2018) (cit. on p. 1).

[6] M. Hörmann and K. P. Schmidt, "Dynamic structure factor of heisenberg bilayer dimer phases in the presence of quenched disorder and frustration", Phys. Rev. B **102**, 094427 (2020) (cit. on p. 1).

[7] R. B. Griffiths, "Nonanalytic behavior above the critical point in a random ising ferromagnet", Phys. Rev. Lett. **23**, 17 (1969) (cit. on pp. 1, 7).

[8] B. M. McCoy, "Incompleteness of the critical exponent description for ferromagnetic systems containing random impurities", Phys. Rev. Lett. **23**, 383 (1969) (cit. on pp. 1, 7).

[9] A. B. Harris, "Effect of random defects on the critical behaviour of ising models", Journal of Physics C: Solid State Physics **7**, 1671 (1974) (cit. on pp. 1, 6).

[10] P. Pfeuty, "An exact result for the 1d random ising model in a transverse field", Physics Letters A **72**, 245 (1979) (cit. on pp. 1, 11, 38, 39, 50).

[11] D. S. Fisher, "Random transverse field ising spin chains", Phys. Rev. Lett. **69**, 534 (1992) (cit. on pp. 1, 33, 34, 38, 39, 45, 50).

[12] T. Vojta, "Phases and phase transitions in disordered quantum systems", in AIP conference proceedings (2013) (cit. on pp. 1, 3–8).

[13] A. W. Sandvik, "Stochastic series expansion method for quantum Ising models with arbitrary interactions", Phys. Rev. E **68**, 056701 (2003) (cit. on pp. 2, 18, 21, 50).

[14] S. Sachdev, *Quantum Phase Transitions*, 2nd ed. (Cambridge University Press, 2011) (cit. on pp. 3–5, 10, 29).

[15] A. Weinrib and B. I. Halperin, "Critical phenomena in systems with long-range-correlated quenched disorder", Phys. Rev. B **27**, 413 (1983) (cit. on p. 6).

[16] J. T. Chayes, L. Chayes, D. S. Fisher, and T. Spencer, "Finite-size scaling and correlation lengths for disordered systems", Phys. Rev. Lett. **57**, 2999 (1986) (cit. on pp. 7, 33).

[17] F. Igloi and C. Monthus, "Strong disorder RG approach of random systems", Physics Reports **412**, 277 (2005) (cit. on pp. 8, 31–33, 49).

[18] E. Ising, "Beitrag zur Theorie des Ferromagnetismus", Zeitschrift für Physik **31**, 253 (1925) (cit. on p. 9).

[19] P. de Gennes, "Collective motions of hydrogen bonds", Solid State Communications **1**, 132 (1963) (cit. on p. 9).

[20] L. Onsager, "Crystal statistics. i. a two-dimensional model with an order-disorder transition", Phys. Rev. **65**, 117 (1944) (cit. on p. 10).

[21] R. Moessner and S. L. Sondhi, "Ising models of quantum frustration", Phys. Rev. B **63** (2001) (cit. on p. 10).

[22] Villain, J., Bidaux, R., Carton, J.-P., and Conte, R., "Order as an effect of disorder", J. Phys. France **41**, 1263 (1980) (cit. on p. 10).

[23] M. Powalski, K. Coester, R. Moessner, and K. P. Schmidt, "Disorder by disorder and flat bands in the kagome transverse field ising model", Phys. Rev. B **87**, 054404 (2013) (cit. on p. 10).

[24] P. Pfeuty, "The one-dimensional ising model with a transverse field", Annals of Physics **57**, 79 (1970) (cit. on p. 12).

[25] S. Funk, *Lecture: Methods of data analysis*, Friedrich Alexander Universität Erlangen, 2019 (cit. on p. 16).

[26] S. Humeniuk, "Quantum monte carlo studies of strongly correlated systems for quantum simulators", PhD thesis (2018) (cit. on pp. 17–19, 25).

[27] X. Zhu, *Lecture notes in Advanced Artificial Intelligence: Markov Chain Monte Carlo*, University of Wisconsin-Madison, 2011 (cit. on p. 17).

[28] A. W. Sandvik, "A generalization of handscomb's quantum monte carlo scheme-application to the 1d hubbard model", Journal of Physics A: Mathematical and General **25**, 3667 (1992) (cit. on p. 18).

[29] D. C. Handscomb, "The monte carlo method in quantum statistical mechanics", Mathematical Proceedings of the Cambridge Philosophical Society **58**, 594 (1962) (cit. on p. 18).

[30] A. W. Sandvik, "Computational studies of quantum spin systems", in AIP conference proceedings, Vol. 1297, 1 (American Institute of Physics, 2010), pp. 135–338 (cit. on pp. 18, 19, 21, 25, 26, 28).

[31] A. Langheld, "Quantum-critical properties of the one-dimensional long-range transverse-field Ising model extracted by quantum Monte-Carlo simulations", MA thesis (2021) (cit. on pp. 18, 25, 28).

[32] J. A. Koziol, "Quantum criticality of the long-range transverse-field Ising model on the square lattice - A quantum Monte Carlo study", MA thesis (2021) (cit. on pp. 18, 25).

[33] A. J. Walker, "An efficient method for generating discrete random variables with general distributions", ACM Trans. Math. Softw. **3**, 253 (1977) (cit. on p. 23).

[34] C. Seshadhri, *Lecture notes to randomized algorithms: Walker's alias method*, 2020 (cit. on p. 23).

[35] A. W. Sandvik and J. Kurkijärvi, "Quantum monte carlo simulation method for spin systems", Phys. Rev. B **43**, 5950 (1991) (cit. on p. 27).

[36] A. W. Sandvik, "Classical percolation transition in the diluted two-dimensional $S = \frac{1}{2}$ heisenberg antiferromagnet", Phys. Rev. B **66**, 024418 (2002) (cit. on pp. 30, 50).

[37] M. E. Fisher and M. N. Barber, "Scaling theory for finite-size effects in the critical region", Phys. Rev. Lett. **28**, 1516 (1972) (cit. on p. 31).

[38] A. Hankey and H. E. Stanley, "Systematic application of generalized homogeneous functions to static scaling, dynamic scaling, and universality", Phys. Rev. B **6**, 3515 (1972) (cit. on p. 31).

[39] T. R. Kirkpatrick and D. Belitz, "Exponent relations at quantum phase transitions with applications to metallic quantum ferromagnets", Phys. Rev. B **91**, 214407 (2015) (cit. on p. 32).

[40] K. Binder, "Finite size effects on phase transitions", Ferroelectrics **73**, 43 (1987) (cit. on p. 32).

[41] Monthus, C. and Garel, T., "Distribution of pseudo-critical temperatures and lack of self-averaging in disordered poland-scheraga models with different loop exponents", Eur. Phys. J. B **48**, 393 (2005) (cit. on pp. 32, 34, 50).

[42] F. Iglói, Y.-C. Lin, H. Rieger, and C. Monthus, "Finite-size scaling of pseudocritical point distributions in the random transverse-field ising chain", Phys. Rev. B **76**, 064421 (2007) (cit. on pp. 32, 33, 38–40, 50).

[43] I. A. Kovács and F. Iglói, "Critical behavior and entanglement of the random transverse-field ising model between one and two dimensions", Phys. Rev. B **80**, 214416 (2009) (cit. on p. 32).

[44] I. A. Kovács and F. Iglói, "Renormalization group study of the two-dimensional random transverse-field ising model", Phys. Rev. B **82**, 054437 (2010) (cit. on pp. 32, 38, 42–45, 50).

[45] F. Pázmándi, R. T. Scalettar, and G. T. Zimányi, "Revisiting the theory of finite size scaling in disordered systems: ν can be less than $2/d$", Phys. Rev. Lett. **79**, 5130 (1997) (cit. on p. 33).

[46] O. Motrunich, S.-C. Mau, D. A. Huse, and D. S. Fisher, "Infinite-randomness quantum ising critical fixed points", Phys. Rev. B **61**, 1160 (2000) (cit. on p. 33).

[47] P. Weinberg and M. Bukov, "QuSpin: a Python package for dynamics and exact diagonalisation of quantum many body systems part I: spin chains", SciPost Phys. **2**, 003 (2017) (cit. on p. 38).

[48] C. Monthus and T. Garel, "The random transverse field ising model in d = 2: analysis via boundary strong disorder renormalization", Journal of Statistical Mechanics: Theory and Experiment **2012**, P09016 (2012) (cit. on pp. 38, 42, 43, 50).

[49] A. P. Young and H. Rieger, "Numerical study of the random transverse-field ising spin chain", Phys. Rev. B **53**, 8486 (1996) (cit. on pp. 39, 48, 51).

[50] A. Crisanti and H. Rieger, "Random-bond ising chain in a transverse magnetic field: a finite-size scaling analysis", Journal of Statistical Physics **77**, 1087 (1994) (cit. on p. 39).

[51] I. A. Kovács, personal communication, July 29, 2022 (cit. on p. 43).

[52] F. Iglói and C. Monthus, "Strong disorder RG approach – a short review of recent developments", The European Physical Journal B **91** (2018) (cit. on p. 43).

[53] S.-k. Ma, C. Dasgupta, and C.-k. Hu, "Random antiferromagnetic chain", Phys. Rev. Lett. **43**, 1434 (1979) (cit. on p. 44).

[54] C. Pich, A. P. Young, H. Rieger, and N. Kawashima, "Critical behavior and griffiths-mccoy singularities in the two-dimensional random quantum ising ferromagnet", Phys. Rev. Lett. **81**, 5916 (1998) (cit. on pp. 48, 51).

Danksagung

Zunächst möchte ich mich bei Kai Phillip Schmidt für die sehr gute Betreuung bedanken. Ich habe mich, wie schon während der Bachelorarbeit, nie verloren gefühlt und konnte aus den zahlreichen Treffen sehr viel mitnehmen. Ein großer Dank gilt auch Anja Langheld, Jan Koziol und Max Hörmann für die anregenden Diskussionen und das Beantworten so vieler Fragen. Ohne diese Unterstützung wäre diese Arbeit nicht möglich gewesen.
Auch beim Rest der Arbeitsgruppe und des Lehrstuhls möchte ich mich für die tolle Atmosphäre bei Seminaren, Kaffeepausen, Mittagessen, Saufest und auch bei Treffen außerhalb der Uni bedanken.
Meiner Familie bin ich dankbar für die uneingeschränkte Unterstützung meines Studiums. Auch möchte ich mich bedanken bei der Hanns-Seidel Stiftung für die ideelle und finanzielle Förderung meines Studiums. Die numerischen Rechnungen in dieser Arbeit wurden auf dem Emmy-Cluster des Zentrums für Nationales Hochleistungsrechnen Erlangen (NHR@FAU) des Regionalen Rechenzentrums Erlangen (RRZE) durchgeführt.

Eigenständigkeitserklärung

Hiermit bestätige ich, dass ich diese Arbeit selbstständig und nur unter Verwendung der angegebenen Hilfsmittel angefertigt habe.

Erlangen, den 30.11.2022 Calvin Krämer